p53 down-regulates SARS coronavirus replication and is targeted by the SARS-unique domain and PL^{pro} via E3 ubiquitin ligase RCHY1

Yue Ma-Lauer[a,b], Javier Carbajo-Lozoya[b], Marco Y. Hein[c,1], Marcel A. Müller[d], Wen Deng[e], Jian Lei[a], Benjamin Meyer[d], Yuri Kusov[a], Brigitte von Brunn[b], Dev Raj Bairad[b], Sabine Hünten[f], Christian Drosten[d], Heiko Hermeking[f], Heinrich Leonhardt[e], Matthias Mann[c], Rolf Hilgenfeld[a], and Albrecht von Brunn[b,2]

[a]Institute of Biochemistry, Center for Structural and Cell Biology in Medicine, University of Lübeck and German Center for Infection Research, partner site Luebeck, 23538 Luebeck, Germany; [b]Max-von-Pettenkofer Institute, Ludwig-Maximilians-University Munich and German Center for Infection Research (DZIF), partner site Munich, 80336 Munich, Germany; [c]Department of Proteomics and Signal Transduction, Max-Planck Institute of Biochemistry, 82152 Martinsried, Germany; [d]Institute of Virology, University of Bonn Medical Centre and German Center for Infection Research, partner site Bonn, 53127 Bonn, Germany; [e]Department of Biology and Center for Integrated Protein Science, Ludwig-Maximilians-University Munich, 82152 Planegg-Martinsried, Germany; and [f]Experimental and Molecular Pathology, Institute of Pathology, Ludwig-Maximilians-University Munich, 80337 Munich, Germany

Edited by Kenneth I. Berns, University of Florida College of Medicine, Gainesville, FL, and approved June 27, 2016 (received for review March 15, 2016)

Highly pathogenic severe acute respiratory syndrome coronavirus (SARS-CoV) has developed strategies to inhibit host immune recognition. We identify cellular E3 ubiquitin ligase ring-finger and CHY zinc-finger domain-containing 1 (RCHY1) as an interacting partner of the viral SARS-unique domain (SUD) and papain-like protease (PL^{pro}), and, as a consequence, the involvement of cellular p53 as antagonist of coronaviral replication. Residues 95–144 of RCHY1 and 389–652 of SUD (SUD-NM) subdomains are crucial for interaction. Association with SUD increases the stability of RCHY1 and augments RCHY1-mediated ubiquitination as well as degradation of p53. The calcium/calmodulin-dependent protein kinase II delta (CAMK2D), which normally influences RCHY1 stability by phosphorylation, also binds to SUD. In vivo phosphorylation shows that SUD does not regulate phosphorylation of RCHY1 via CAMK2D. Similarly to SUD, the PL^{pro}s from SARS-CoV, MERS-CoV, and HCoV-NL63 physically interact with and stabilize RCHY1, and thus trigger degradation of endogenous p53. The SARS-CoV papain-like protease is encoded next to SUD within nonstructural protein 3. A SUD–PL^{pro} fusion interacts with RCHY1 more intensively and causes stronger p53 degradation than SARS-CoV PL^{pro} alone. We show that p53 inhibits replication of infectious SARS-CoV as well as of replicons and human coronavirus NL63. Hence, human coronaviruses antagonize the viral inhibitor p53 via stabilizing RCHY1 and promoting RCHY1-mediated p53 degradation. SUD functions as an enhancer to strengthen interaction between RCHY1 and nonstructural protein 3, leading to a further increase in in p53 degradation. The significance of these findings is that down-regulation of p53 as a major player in antiviral innate immunity provides a long-sought explanation for delayed activities of respective genes.

p53 antiviral activity | SARS-CoV SUD | papain-like protease | E3 ubiquitin ligase RCHY1 | coronavirus replication

The global outbreak of severe acute respiratory syndrome coronavirus (SARS-CoV) in 2003 caused 774 deaths among 8,098 infected individuals, although human coronaviruses (HCoVs) had always been regarded relatively harmless until then (1, 2). To date, six coronaviruses (CoVs) are known to infect humans; these are HCoV-229E and HCoV-NL63 belonging to the genus *Alphacoronavirus* as well as SARS-CoV, Middle East respiratory syndrome CoV (MERS-CoV), HCoV-HKU1, and HCoV-OC43 of the *Betacoronavirus* genus. MERS-CoV is another highly pathogenic coronavirus connected with an even higher case/fatality rate. Despite a decade of research efforts, there are neither approved antiviral treatments either specific for SARS-CoV or with a broad-spectrum profile for all human coronaviruses, nor any vaccine available (2–4). Therefore, it is necessary to further study coronavirus–host relations to discover new targets and signaling pathways for antiviral intervention. Applying high-throughput yeast-2-hybrid (Y2H) methodologies to screen for important virus–host protein–protein interactions (PPIs), we identified ring-finger and CHY zinc-finger domain-containing 1 (RCHY1) and calcium/calmodulin-dependent protein kinase II delta (CAMK2D) as two interacting partners of the SARS-unique domain (SUD), which is part of SARS-CoV nonstructural protein 3 (Nsp3). Containing various subdomains [ubiquitin-like (Ubl) globular fold, acidic domain, catalytically active ADP ribose-1″-phosphatase (X-domain), SUD, Ubl, catalytically active papain-like protease (PL^{pro}) domain, nucleic acid-binding domain, G2M marker domain, two predicted double-pass transmembrane domains, a putative metal binding region, Y domain of unknown function], Nsp3 protein represents the largest Nsp of SARS-CoV (5) and plays an essential role for the formation of viral replication complexes. Two macrodomains of SUD (SUD-N and, in particular, SUD-M) have been shown to bind oligo(G) nucleotides (both deoxynucleotides and ribonucleotides) that are able to form G-quadruplexes (6). Interestingly,

Significance

Severe acute respiratory syndrome coronavirus (SARS-CoV) is one of the most pathogenic human coronaviruses. Virulence is reflected in the molecular interplay between virus and host cells. Here we show a strategy of how SARS-CoV antagonizes the host antiviral factor p53, which impairs viral replication. The papain-like protease of the nonstructural protein 3 of SARS-CoV and other coronaviruses physically interact with and stabilize E3 ubiquitin ligase ring-finger and CHY zinc-finger domain-containing 1 (RCHY1), thereby augmenting RCHY1-mediated degradation of p53. The SARS-unique domain (SUD) enhances these effects. Knockout of p53 promotes replication of SARS-CoV replicons and of infectious virus. Taken together we identify cellular p53 as antiviral measure of coronavirus-infected cells, which is counteracted via the stabilization of RCHY1 by viral SUD and papain-like protease (PL^{pro}) proteins and via ubiquitination of p53.

Author contributions: Y.M.-L., J.C.-L., M.Y.H., M.A.M., and A.v.B. designed research; Y.M.-L., J.C.-L., M.Y.H., M.A.M., W.D., J.L., B.M., B.v.B., and D.R.B. performed research; J.L., B.M., Y.K., S.H., C.D., H.H., H.L., M.M., and R.H. contributed new reagents/analytic tools; Y.M.-L., J.C.-L., M.Y.H., M.A.M., W.D., J.L., B.v.B., D.R.B., H.L., and A.v.B. analyzed data; and Y.M.-L. and A.v.B. wrote the paper.

The authors declare no conflict of interest.

This article is a PNAS Direct Submission.

Freely available online through the PNAS open access option.

[1]Present address: Cellular and Molecular Pharmacology, University of California, San Francisco, CA 94158.

[2]To whom correspondence should be addressed. Email: vonbrunn@mvp.uni-muenchen.de.

This article contains supporting information online at www.pnas.org/lookup/suppl/doi:10.1073/pnas.1603435113/-/DCSupplemental.

amino acid residues of SUD-M that have been shown to be involved in G-quadruplex binding (6) are also essential for the function of the domain in SARS-CoV replication and transcription (7). PL^{pro} (corresponding to Nsp3 residues 720–1039) is the C-terminal neighbor to the SUD. PL^{pro} and 3C-like proteinase ($3CL^{pro}$) process the viral replicase polyproteins into 16 replicase proteins. Many CoVs encode two Papain-like proteases (PLPs) [PLP1 (cleaving Nsp1/Nsp2 and Nsp2/Nsp3), PLP2 (cleaving Nsp3/Nsp4)] within Nsp3. SARS-CoV PL^{pro} and most of other CoV PL^{pro}s display deubiquitinating and deISGylating activities, thus acting as IFN antagonists and contributing to evasion of innate immune response.

RCHY1 is an E3 ubiquitin ligase mediating proteasomal degradation of its target proteins; its targets include the tumor proteins p53, p63, and p73 (8–10). RCHY1 regulates cell-cycle progression and is inducible by p53 (8, 11); it also forms a homodimer and has self-ubiquitination activity (12). RCHY1 is a short-lived protein. Inhibition of RCHY1 ubiquitination via interaction with measles virus phosphoprotein can enhance the stability of RCHY1 (13). In addition, phosphorylation by cyclin-dependent kinase 9 (CDK9) or CAMKII can also regulate the stability of RCHY1. Phosphorylation by CAMKII at Thr154/Ser155 increases instability of RCHY1 and impairs the E3 ubiquitin ligase activity of RCHY1 toward p53 (14).

CAMK2D belongs to the calcium/calmodulin-dependent serine/threonine protein kinase II (CAMKII) family involved in many signaling pathways. CAMKII is a holoenzyme composed of CAMK2A/2B/2G/2D isoforms (15). These have very similar structures, including an N-terminal kinase domain, a central regulatory domain with a calmodulin-binding region, and a C-terminal association domain (15–17). Important substrates of CAMKII include RCHY1 and signal transducer and activator of transcription 1 (STAT1). CAMKII impairs the E3 ligase activity of RCHY1 via phosphorylation (14).

p53 regulates a plethora of target genes that mediate tumor suppression by inducing multiple processes such as cell-cycle arrest, DNA repair, apoptosis, and senescence (18, 19). The proteasomal degradation of p53 is regulated by several E3 ubiquitin ligases such as RCHY1 and MDM2 (8, 20, 21). RCHY1 binds to the central region of p53, ubiquitinates p53, and promotes p53 degradation independently of MDM2 (8). Like RCHY1, MDM2 is also a zinc finger and RING domain-containing E3 ubiquitin ligase (22). High levels of MDM2 induce polyubiquitination and degradation of p53, whereas low levels of MDM2 lead to monoubiquitination and nuclear export of p53 (23). CDK9 phosphorylates RCHY1 at Ser211/Thr217 and MDM2 at Ser395, causing degradation of RCHY1 and attenuated activity of MDM2 toward p53, respectively (24, 25). p53 can also be directly phosphorylated by CDK9 at Ser392, leading to p53 accumulation (26). In addition to its tumor suppressive activity, p53 also serves as host defense molecule during viral infection (27). Notably, p53 was identified by its interaction with SV40 large T antigen (28). Overexpression of p53 reduces HIV-1 replication via preventing phosphorylation of RNA polymerase II and consequently establishing a delayed RNA polymerase II complex at the LTR of HIV-1 (29). A recent study reported that ectopic expression of HCoV-NL63 PLP2 promotes p53 degradation by interaction with the cellular ubiquitin ligase MDM2 and that p53 exhibits antiviral activity on the replication of Sendai virus (30). Furthermore, p53 functions as an antiviral factor against influenza A virus (31). To antagonize the negative effect of p53, some viruses have evolved strategies to induce p53 degradation. Epstein–Barr virus (EBV) applies a double strategy to counteract p53. First, EBV nuclear antigen 3C deubiquitinates and stabilizes MDM2, thereby enhancing ubiquitination and degradation of p53 (32). Second, during the lytic infection of EBV, p53 is phosphorylated and incapable of interacting with MDM2. However, the viral BZLF1 protein can interact with p53 and subsequently recruit p53, especially phosphorylated p53, to ECS E3 ubiquitin ligase complex for ubiquitin-mediated degradation (33).

We have recently established a SARS-CoV–host interactome by screening interactions of individual viral proteins against human cDNA libraries, leading to the identification of important cellular pathways and targets for the prevention of CoV replication (34). In the present study, we investigate the SUD–CAMK2D as well as SUD–RCHY1 interactions, identify p53 as a negative regulator of CoV replication, and characterize the RCHY1-dependent mechanism for SARS-CoV to abolish p53 antiviral activity.

Results

SUD Interacts with RCHY1 and CAMK2D in Vivo. Studying virus–host interactions, we have recently performed Y2H screens of a complete SARSCoV ORF collection (ORFeome) with human cDNA libraries (34). Several E3 ubiquitin protein ligases including RCHY1 were identified as interacting partners of SUD. Independently, plasmids expressing an ectopic GFP–SUD fusion were transfected into HEK293 cells. Together with its host-binding partners, the GFP–SUD fusion protein was subsequently enriched with a GFP-trap consisting of beads coated with anti-GFP antibodies. After quantitative mass-spectrometry analysis of the proteins bound to the beads (35, 36), RCHY1 showed up again as an interacting partner of SUD (Fig. 1 *A*–*C*). In addition, CAMK2D was also identified to bind to SUD in the same assay. RCHY1–SUD interaction was further confirmed by fluorescence-3-hybrid assay (Fig. S1). Most interestingly, RCHY1 is a substrate of CAMKII (14).

To confirm that SUD also binds to those novel partners in vivo, split-YFP protein–protein interaction assays were carried out in human living cells (HEK-293). SUD and its interacting candidates were fused to the C-terminal (YFP^C) and N-terminal (YFP^N) YFP fragments, respectively. If SUD binds to a tested candidate in this assay, the N-terminal and C-terminal YFP fragments will assemble, leading to fluorescence emission (37). As a result, SUD was demonstrated to bind to both RCHY1 and CAMK2D in the cytosol of HEK293 living cells (Fig. 1 *D* and *E*).

CAMKII isoforms can phosphorylate RCHY1 at T154/S155 in vitro (14), but a physical interaction between RCHY1 and CAMK2D has never been examined in vivo. For this reason, a split-YFP assay was performed. However, no clear YFP signal representing association of RCHY1 and CAMK2D was detected. The in vivo expression level of RCHY1 was subsequently found to be extremely low in the presence of CAMK2D, compared with the expression level in the presence of SUD. Alternatively, the RCHY1–CAMK2D interaction was tested by a highly sensitive coimmunoprecipitation (coIP) assay. As shown in Fig. 1 *F* and *G*, the SUD–RCHY1 and SUD–CAMK2D interactions were further confirmed (Fig. 1*F*, compare lanes 2 and 4 with lane 1; Fig. 1*G*, compare lanes 6 and 5). Furthermore, the RCHY1–CAMK2D interaction was detected (Fig. 1*F*, compare lane 3 and 4 with lane 1). Negative controls (lane 1 in Fig. 1*F* and lane 5 in Fig. 1*G*) showed no unspecific binding of CAMK2D–HA or SUD–RFP to the GFP-trap. In conclusion, there is direct physical interaction between each pair of proteins among CAMK2D, RCHY1, and SUD.

RCHY1 Residues 95–144 Bind to SUD. The RCHY1 protein as an interacting partner of SUD consists of 261 aa residues. The N-terminal fragment comprising residues 1–94 contains a CHY zinc-finger domain (residues 20–94) that is responsible for binding to calmodulin (14). The C-terminal fragment comprising residues 145–261 contains a RING-finger domain (residues 145–186) with intrinsic E3 ubiquitin ligase activity and a zinc ribbon (residues 190–250). The middle region of RCHY1 comprising residues 120–137 is required for binding to tumor protein p53 and to CDK9 (8, 24). Phosphorylation by CAMKII at T154/S155 or by CDK9 at S211/T217 enhances self-ubiquitination of RCHY1 and shortens its half-life (14, 24). A schematic domain presentation of RCHY1 is shown in Fig. 2*A*.

To determine which region is crucial for interaction with SUD, we cloned two truncated RCHY1 fragments into split-YFP destination vectors and tested their interactions with SUD. One fragment contained residues 1–144 and was thus lacking the RING-finger domain and the zinc ribbon; the other contained residues 95–261 and was devoid of the calmodulin-binding region (Fig. 2*A*). Interestingly, both truncated RCHY1 fragments interacted with SUD (Fig. 2*B*). The region in common between these two fragments, residues 95–144, was consequently supposed to be required for binding to SUD. Indeed, it was subsequently demonstrated that the RCHY1 fragment 95–144 interacted with SUD in the cytosol of HEK293 cells (Fig. 2*B*).

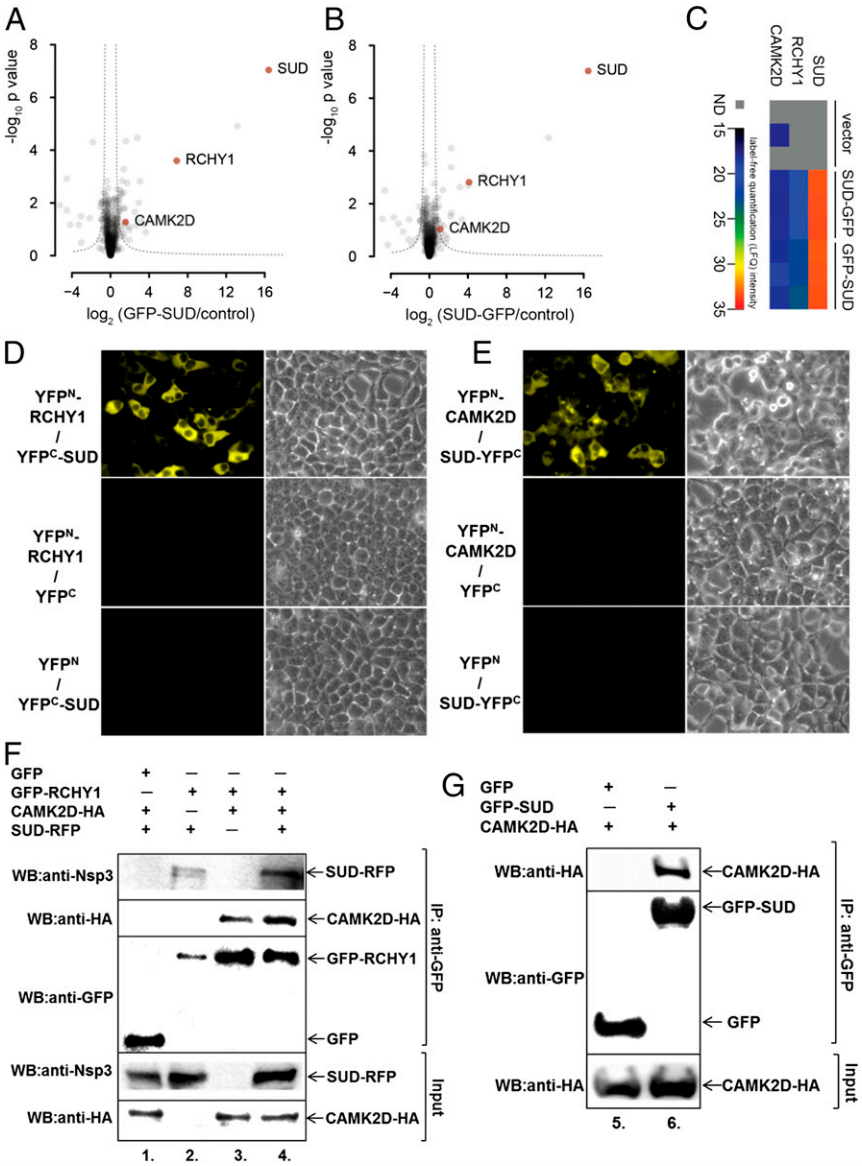

Fig. 1. Interactions among SUD, RCHY1, and CAMK2D. Affinity-enrichment mass spectrometry screen (*A*–*C*): SUD with a C- or N-terminal GFP tag was recombinantly expressed in HEK293 cells and enriched from cell lysates using GFP-trap agarose beads (ChromoTek). Volcano plots show enrichment factors of all quantified proteins in C-terminally (*A*) or N-terminally (*B*) tagged SUD-expressing samples over vector-only controls, plotted against *P* values determined from a two-sample *t* test between three replicates each. Significance curves were determined as described (36) using $c = 0.5$ and $x_0 = 0.5$ cutoff parameters. (*C*) Label-free quantification intensities of selected proteins across all samples. To calculate enrichment factors, missing quantifications were imputed with noise simulating the detection limit (35). (*D*) Split YFP: YFP^N (YFP^N-terminal fragment, amino acids 1–155) was fused to the N terminus of RCHY1, and YFP^C (YFP^C-terminal fragment, amino acids 156–239) was fused to the N terminus of SUD. At 24 h after cotransfection of both plasmids into HEK-293 cells, strong YFP signal was detected in the cytosol. Negative controls are YFP^N–RCHY1 in combination with YFP^C vector and YFP^C–SUD in combination with YFP^N vector. (*E*) Split YFP: YFP^N was fused to the N terminus of CAMK2D, and YFP^C was fused to the C terminus of SUD. At 24 h after cotransfection, clear YFP signal was detected in the cytosol of HEK293 cells. (*F*) Co-IP: plasmids expressing the indicated genes were transfected into HEK293 cells grown in 10-cm dishes. At 24 h after transfection, cells were lysed and the lysates were purified with GFP-trap consisting of agarose beads coated with anti-GFP antibodies. IP samples were analyzed by 12% (wt/vol) SDS/PAGE and Western blotting (WB) with anti–SARS-CoV Nsp3, anti-HA, and anti-GFP antibodies. (*G*) Co-IP: plasmids expressing CAMK2D–HA fusion together with plasmids expressing GFP or GFP–SUD were cotransfected into HEK293 cells grown in 10-cm dishes. At 24 h after transfection, cells were lysed. The lysates were purified with GFP-trap and subsequently analyzed by WB with anti-HA and anti-GFP antibodies.

Of note, the RCHY1 binding sites for p53 and CDK9 are within this region (8, 24).

SUD-NM Interacts with RCHY1. SUD is located between the X-domain and the PL^{pro} domain of SARS-CoV Nsp3 (Fig. S2*A*); it consists of three subdomains: SUD-N, SUD-M, and SUD-C. SUD-N and, in particular, SUD-M have been demonstrated to bind oligo(G) nucleotides capable of forming G-quadruplexes (6). In addition, SUD-C exhibits RNA-binding activity (38). The interaction between RCHY1 and diverse SUD subdomain fragments was tested by split-YFP microscopy (Fig. S2*B*). SUD-NM did bind to RCHY1, whereas neither SUD-N nor SUD-M alone did. SUD-MC did not bind to RCHY1 either. The results indicate that both SUD-N and SUD-M are indispensable for the interaction with RCHY1.

MERS-CoV is another highly pathogenic coronavirus. The MERS Nsp3 contains a homolog to SUD-MC, but not to SUD-N (Fig. S3). The interaction between RCHY1 and MERS-MC (homologous to SUD-MC) was also analyzed by split-YFP fluorescence microscopy. Consistent with the lacking interaction between SUD-MC and RCHY1, MERS-MC did not bind to RCHY1 (Fig. S2*C*).

SUD Augments Ubiquitination of p53. As shown previously, the E3 ubiquitin protein ligase RCHY1 physically interacts with SUD. Because p53 is subject to ubiquitination by RCHY1, both in vivo and in vitro (8), we examined whether binding to SUD influences the E3 ubiquitin ligase activity of RCHY1. As mentioned previously, the region of RCHY1 involved in binding to p53 is within the RCHY1 fragment (residues 95–144) that binds to SUD. Therefore, we first assumed SUD to compete with the RCHY1–p53 interaction and consequently impair RCHY1-mediated ubiquitination of p53. However, the in vivo ubiquitination assay revealed that SUD dramatically promoted the ubiquitination of p53 (Fig. 3*A*). The negative control (Fig. 3*A*, lane 1) shows that GFP was not ubiquitinated by RCHY1. Thus, the multiple bands appearing in the anti-HA blot of Fig. 3*A*, lane 2, only represent p53 ubiquitination; compared with lane 2, lane 3 shows that SUD strongly augmented ubiquitination of p53.

As shown in Fig. S2*A*, the PL^{pro} domain occurs next to the C terminus of the SUD within SARS–CoV Nsp3. The PL^{pro} releases the nonstructural proteins Nsp1, Nsp2, and Nsp3 from the viral polyproteins. In addition to being a protease, PL^{pro} possesses deubiquitinating (DUB) and deISGylating activities (39, 40). Initially, we thought that SUD promoting p53 ubiquitination was in conflict with the DUB activity of PL^{pro}. The SARS–CoV PL^{pro} and the SUD–PL^{pro} fusion were therefore cloned to test whether p53 is a substrate of the PL^{pro}. The in vivo ubiquitination assay demonstrated that the PL^{pro} was not able to deubiquitinate p53 (Fig. 3*B*). The two anti-HA

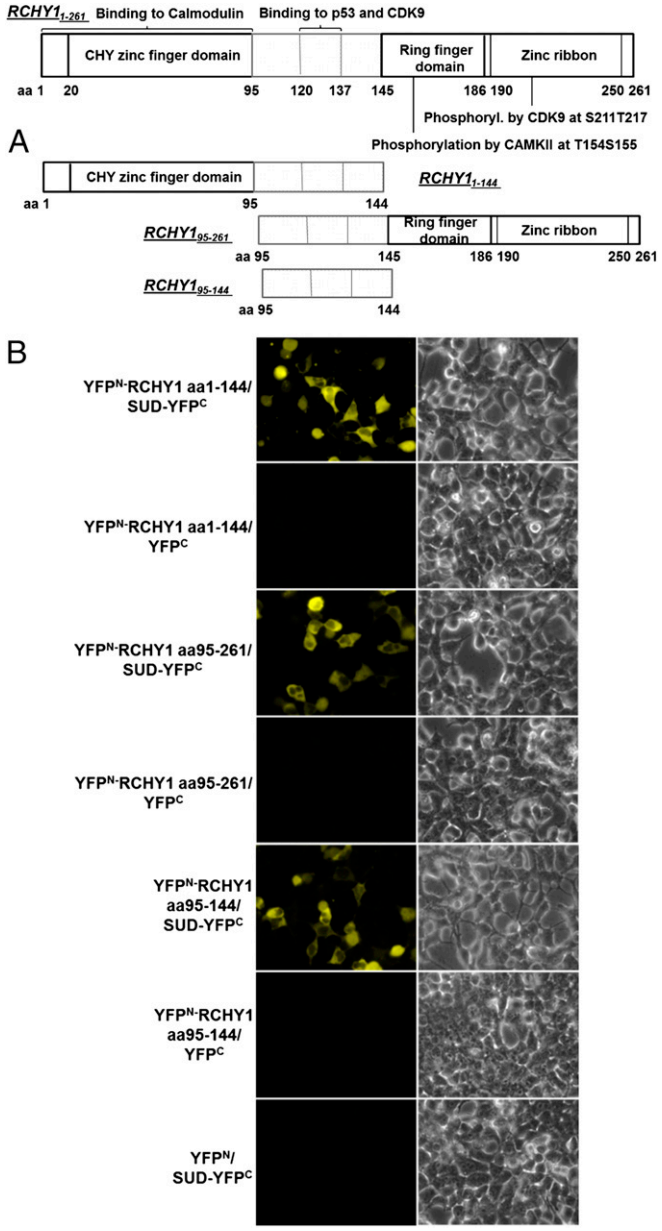

Fig. 2. RCHY1 amino acids 95–144 and SUD-NM are crucial for interaction. (*A*) Scheme of RCHY1. (*B*) Split YFP: YFP^N was fused to the N terminus of truncated RCHY1 fragments, and YFP^C was fused to the C terminus of SUD. At 24 h after transfection of the expression plasmids into HEK293 cells, YFP signal was examined by fluorescence microscopy.

blots of input and immunoprecipitation samples showed that the PL^{pro} deubiquitinated some endogenous proteins but not p53 (compare lane 4 with lanes 1 and 2 in Fig. 3*B*). Like SUD, the SUD–PL^{pro} fusion protein was also able to augment ubiquitination of p53 (compare lane 3 with lane 2 in Fig. 3*B*). Interestingly, as shown in the anti-Myc blot, the protein level of Myc-YFP^N–RCHY1 was up-regulated by both PL^{pro} and SUD–PL^{pro}.

SUD Does Not Interfere with Phosphorylation of RCHY1. CAMKII phosphorylates RCHY1 at T154/S155 and thereby impairs the E3 ubiquitin ligase activity of RCHY1 toward p53 (14). CAMK2D, as a member of the CAMKII family, binds to RCHY1 (Fig. 1*F*). SUD interacts with both RCHY1 and CAMK2D (Fig. 1). To find out whether SUD interferes with CAMK2D-mediated phosphorylation of RCHY1 (e.g., by blocking the enzymatic domain of CAMK2D or by hiding the phosphorylation sites of RCHY1), an in vivo phosphorylation assay was carried out (Fig. 4*A*); this showed that SUD does not regulate CAMK2D-mediated phosphorylation of RCHY1 (compare lane 3 with lane 2). The anti–phospho-Ser/Thr blot of the immunoprecipitates did not reveal phosphorylation of GFP by CAMK2D (Fig. 4*A*, lane 1); similar phosphorylation intensities of RCHY1 were detected in the absence (lane 2) and presence of SUD (lane 3). Phorbol-12-myristate-13-acetate (PMA) and ionomycin were added to the cells to open the calcium channels on the plasma membrane, in view of the calcium and calmodulin dependence of CAMK2D. In conclusion, the interaction between SUD and CAMK2D does not inhibit the protein kinase activity of CAMK2D toward RCHY1.

SUD Stabilizes RCHY1. Phosphorylation of RCHY1 by CAMKII abrogates the E3 ubiquitin ligase activity of RCHY1 toward p53; it also leads to enhanced self-ubiquitination and instability of RCHY1 (14). However, SUD does not block the phosphorylation of RCHY1 despite the fact that SUD augments ubiquitination of p53. To find out the mechanism of how SUD promotes RCHY1-mediated ubiquitination of p53, the protein level of RCHY1 was examined in the absence and presence of SUD. RCHY1 has a short half-life of ∼3.5 h (14). Therefore, the expression level of the RCHY1–RFP fusion was very weak, despite the presence of the strong CMV promoter (Fig. 4*B*, *Upper*). However, SUD clearly enhanced the protein level of RCHY1–RFP fusion (Fig. 4*B*, *Lower*). Western blot has also demonstrated that SUD leads to accumulation of Myc-YFP^N-RCHY1 (Fig. 4*C*).

SUD–PL^{pro} Forms a Complex with RCHY1 and p53. p53 could be pulled down by RCHY1 in a coIP assay (8). RCHY1 is located in both the nucleus and the cytosol, whereas p53 can also shuttle between these two compartments (14, 41). It has not been reported where RCHY1 and p53 interact with each other. Therefore, we performed a split-YFP assay to answer this question. However, the YFP signal was not detectable due to the low expression level of RCHY1. The RCHY1 fragment 1–144 containing both the SUD and p53 binding sites displayed a much higher expression level. The split-YFP assay revealed that p53 interacts with RCHY1 fragment 1–144 mainly in the nucleus and only to a small extent in the cytosol (Fig. 4*D*). Thus, in the cytosol, RCHY1 can interact with both SUD and p53. To investigate whether p53 and SUD compete for binding to RCHY1, an excessive amount of plasmids ectopically expressing the p53–RFP fusion was cotransfected with YFP^N-RCHY1 and YFP^C-SUD plasmids into HEK293 cells (Fig. 4*E*). As a result, the split-YFP signal representing the interaction between RCHY1 and SUD was not diminished, indicating that there was no competition between p53 and SUD for binding to RCHY1.

Subsequently, we tested whether p53 can form a complex simultaneously with RCHY1 and SUD. To better mimic the real situation of the viral protein interacting with RCHY1 in SARS-CoV–infected cells, the SUD–PL^{pro} fusion protein instead of SUD was applied. p53-GFP was able to pull down SUD–PL^{pro} in the coIP assay only if RCHY1 was also expressed (Fig. 4*F*, compare lane 3 with lane 2); this indicates that p53 forms a complex with RCHY1 and SUD–PL^{pro} but there is no direct interaction between p53 and SUD–PL^{pro}. The negative control (Fig. 4*F*, lane 1) shows no unspecific binding of RCHY1 or SUD–PL^{pro} to the GFP-trap.

CDK9 is another important protein kinase involved in RCHY1–p53 signaling. Similar to CAMK2D, CDK9 phosphorylates RCHY1 and enhances the self-ubiquitination of this protein. However, differently from CAMK2D, CDK9 can directly phosphorylate p53 at Ser392 (24). We therefore tested a possible binding of SUD–PL^{pro} to CDK9 but could not detect any interaction (Fig. 4*F*, lane 4).

PL^{pro} Binds to RCHY1 and Promotes Its Accumulation. To confirm that SUD–PL^{pro} binds to RCHY1 in vivo, plasmids expressing YFP^N-SUD–PL^{pro} and YFP^C–RCHY1 were transfected into HEK293 cells for a split-YFP assay. A vector expressing YFP^N–PL^{pro} was applied as one of the controls. By chance, an interaction between RCHY1 and SARS–CoV PL^{pro} was discovered although the

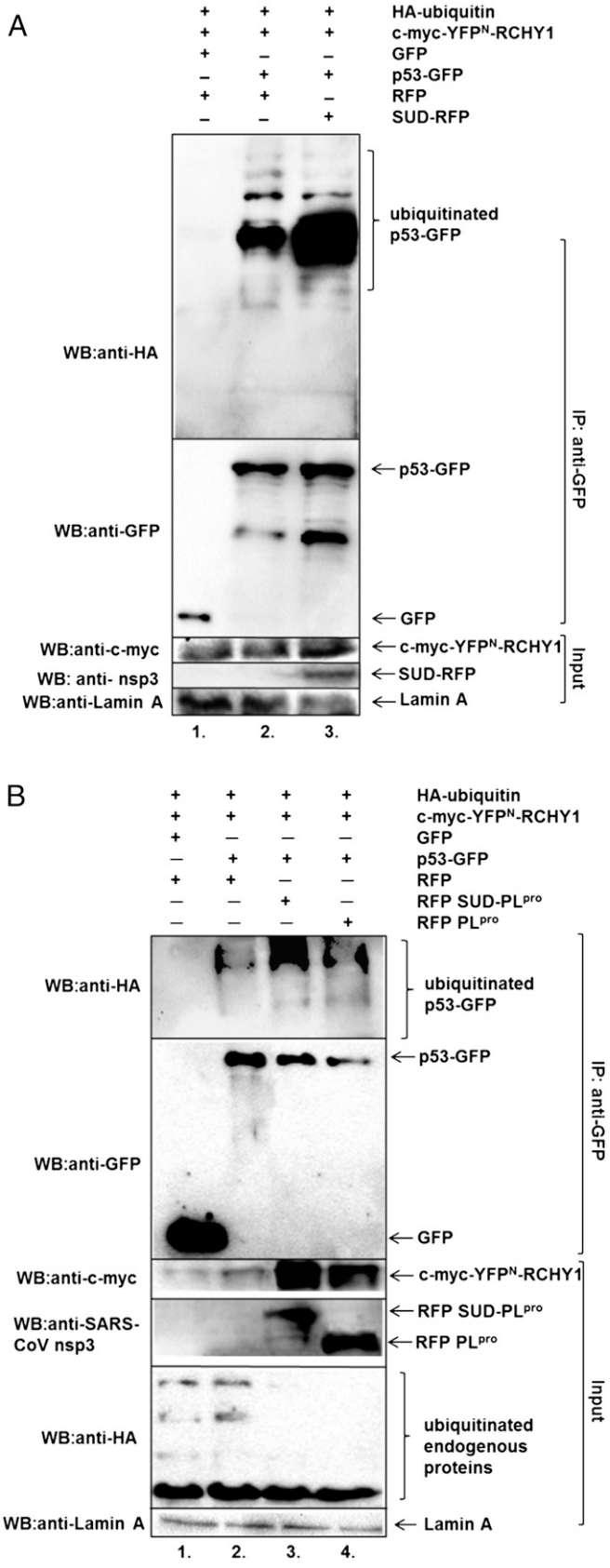

Fig. 3. SUD augments p53 ubiquitination and stabilizes RCHY1. (*A*) Plasmids expressing HA-tagged ubiquitin, c-Myc-tagged YFP^N-RCHY1, GFP or p53–GFP fusion, and RFP or SUD–RFP fusion were cotransfected into HEK293 cells growing in 10-cm dishes. At 24 h after transfection, cells were lysed and the lysates were purified with GFP-trap consisting of beads coated with anti-GFP antibodies. The samples of IP and input were analyzed by 12% (wt/vol) SDS/PAGE and WB with anti-HA, anti-GFP, anti–SARS-CoV Nsp3, anti-Myc, and anti-lamin A antibodies. (*B*) Plasmids expressing indicated proteins were cotransfected into HEK293 cells growing in 10-cm dishes. The in vivo ubiquitination assay was carried out as described in *A*.

interaction was weaker than the interaction between the SUD–PL^{pro} fusion and RCHY1 (Fig. 5*A*).

A coIP assay was subsequently performed to further confirm the binding of PL^{pro} to RCHY1. HA-tagged PL^{pro} was pulled down together with GFP–RCHY1 by the GFP-trap containing beads coated with anti-GFP antibodies (Fig. 5*B*), implying a physical interaction between SARS–CoV PL^{pro} and RCHY1. Similarly to SUD, PL^{pro} also influences the stability of RCHY1 (Fig. 5*C*). Interestingly, both SUD and PL^{pro} led to accumulation of RCHY1 at the protein level but not the mRNA level (Fig. 5*C*, compare lanes 2 and 3 with lane 1). Compared with the SUD–PL^{pro} fusion and PL^{pro}, SUD promoted a slightly higher accumulation of RCHY1 when expressed separately (Fig. 5*C*, compare lane 4 with lanes 2 and 3). Because it is known that viral SARS-CoV PL^{pro} acts as a deubiquitinase on cellular proteins and inhibits innate immune responses, we tested the effect of PL^{pro} on RCHY1 in an in vitro deubiquitination assay (Fig. S4). As RCHY1 was not deubiquitinated by PL^{pro}, the protein must be stabilized by a different, as-yet-unknown mechanism.

SUD–PL^{pro} Leads to Degradation of p53. Ubiquitination of p53 can regulate the protein in many different aspects, such as protease-mediated degradation, degradation-independent nuclear export, and functional alteration (41). To find out the consequence of enhanced p53 ubiquitination promoted by SUD and SUD–PL^{pro}, the endogenous p53 protein level was tested (Fig. 5*D*). Ectopic HA-tagged RCHY1 was transfected into cells as a positive control. Overexpression of RCHY1 resulted in p53 degradation (Fig. 5*D*, compare lane 2 with lane 1). Like the phenotype obtained from the positive control, SUD–PL^{pro} also led to dramatic enhancement of the degradation of p53 (Fig. 5*D*, compare lane 3 with lane 1). Subsequently, PL^{pro} alone was also found to cause p53 degradation (Fig. 5*D*, compare lane 5 with lane 4). Moreover, the SUD–PL^{pro} fusion resulted in further degradation of p53 compared with PL^{pro} alone (Fig. 5*D*, compare lane 6 with lane 5), which indicates that SUD augments p53 degradation.

P53 Inhibits Replication of a SARS-CoV. The tumor suppressor protein p53 has been demonstrated to possess an inhibitory effect on some viruses such as HIV-1 and human papillomavirus (42, 43). Ectopic expression of HCoV-NL63 PLP2 was shown to promote p53 degradation by interaction with the cellular ubiquitin ligase MDM2, leading to reduced replication of Sendai virus (30). However, to our knowledge, a direct effect of p53 on coronavirus replication has not been shown before. To investigate how SARS-CoV benefits from p53 degradation promoted by SUD–PL^{pro}, the influence of p53 on viral growth of SARS-CoV was examined. Human ACE2-transgenic p53-expressing HCT116 cells (HCT116/ACE2 p53$^{+/+}$) as well as p53 knockout cells (HCT116/ACE2 p53$^{-/-}$) were infected with SARS-CoV, and viral replication was monitored by real-time PCR. As shown in Fig. 6, SARS-CoV grew to an ∼1,000-fold higher titer in p53$^{-/-}$ cells compared with p53$^{+/+}$ (Fig. 6*A*). To exclude that differential metabolism or cell growth was responsible for differences in virus replication, cells were infected with a second virus in parallel. Vesicular stomatitis virus (VSV) grew equally well in both p53$^{-/-}$ and p53$^{+/+}$ HCT116/ACE2 cells, suggesting that facilitated growth was SARS-CoV specific (Fig. 6*B*).

Loss-of-function assays were also performed to examine the effect of p53 on replication of the SARS-CoV replicon. The SARS-CoV replicon DNA pBAC-SARS-Rep-R(enilla)Luc (7) and the SARS-CoV replicon RNA in vitro transcribed from pBAC-SARS-Rep-M(etridia)Luc (34) carrying a secreted Metridia luciferase reporter were tested in p53-expressing HCT116

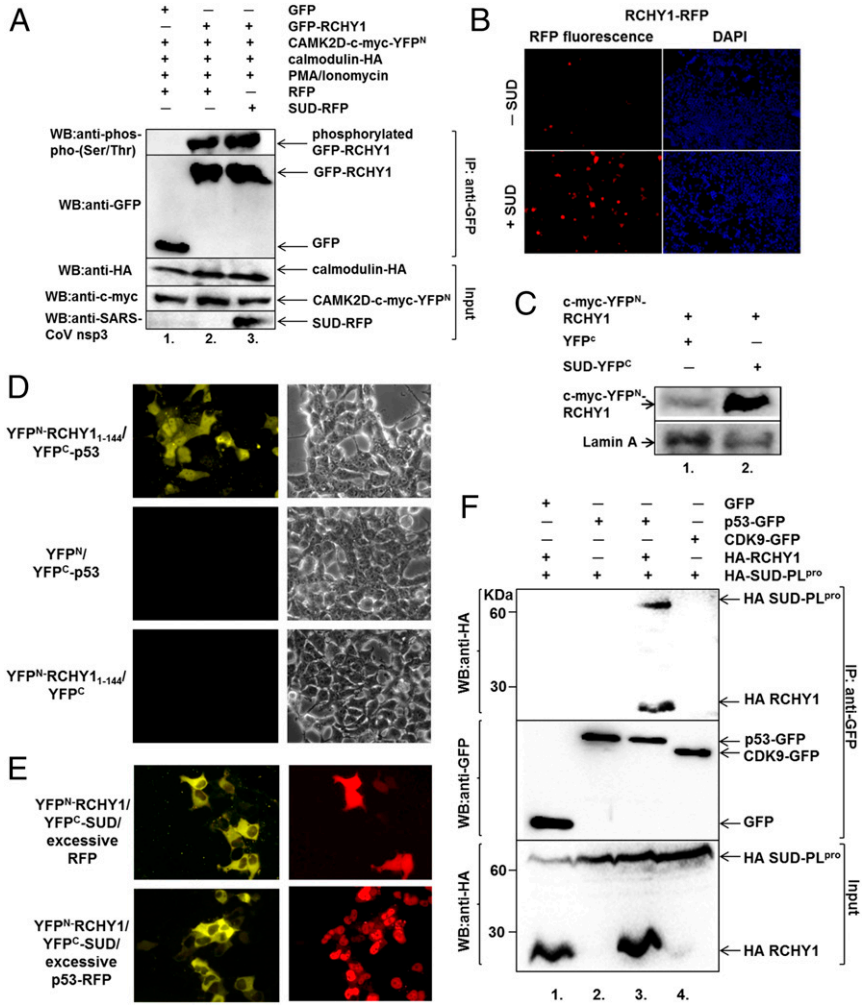

Fig. 4. SUD does not interfere with phosphorylation of RCHY1 and stabilizes it. (*A*) The indicated plasmids were cotransfected into HEK293 cells growing in 10-cm dishes. At 20 h posttransfection, PMA to a final concentration of 20 ng/mL and ionomycin to a final concentration of 1 μM were added to the cells. Two hours after the treatment, cells were lysed and the lysates were purified with GFP-trap. The samples of IP and input were analyzed by 12% (wt/vol) SDS/PAGE/WB and probed with anti–phospho-Ser/Thr, anti-GFP, anti-HA, anti-Myc, and anti–SARS-CoV Nsp3 antibodies. (*B*) Plasmids expressing RCHY1–RFP and plasmids ectopically expressing SUD were cotransfected into HEK293 cells grown on coverslips in a 24-well plate. At 24 h after transfection, cells were fixed with 2% (wt/vol) paraformaldehyde (PFA) and stained with DAPI. The samples were finally examined with a fluorescent microscope (Leica DM4000 B; 10× objective). A representative area of pictures taken randomly is shown. (*C*) Split-YFP plasmids expressing Myc-YFP^N–RCHY1 and expressing YFP^C or SUD–YFP^C were transfected to HEK293 cells growing in a six-well plate. At 24 h after transfection, cells were lysed. The lysates were Western blotted with anti-Myc and anti-lamin A antibodies. (*D*) YFP^N was fused to the N terminus of RCHY1 amino acids 1–144, and YFP^C was fused to the N terminus of p53. Split-YFP fluorescence microscopy was performed as described before. (*E*) The 300-ng plasmids ectopically expressing RFP or p53-RFP together with 100-ng plasmids expressing YFP^N–RCHY1 and YFP^C–SUD were cotransfected into HEK293 cells growing on coverslips in a 24-well plate. The split-YFP experiment was carried out as described before. (*F*) Indicated plasmids were transfected into HEK293 cells growing in 10-cm culture dishes. The GFP-trap-based coIP was performed as described before.

p53$^{+/+}$ and HCT116 p53–knockout p53$^{-/-}$ cells (44) as well as in a doxycycline (DOX)-dependent p53-inducible cell line SW480 (19) (Fig. 6 *C* and *D*). p53 expression was monitored by Western blot using anti-p53 antibodies in the respective cell lines (Fig. S5). Both of the replicons replicated better in HCT116 p53$^{-/-}$ than in HCT116 p53$^{+/+}$, and better in SW480 without DOX induction than in SW480 with DOX induction. The observed fold differences between the use of replicons and virus infection are attributed to the commonly lower replication efficiencies of coronavirus replicons (>27 kb), because transfection/electroporation efficiencies do not reach 100% of cells. On the contrary, viable virus is much more efficient due to multicycle infection and exponential growth when using low multiplicities of infections (MOIs, 0.001).

To explore the efficiency of genome replication of SARS-CoV replicon under the pressure of p53 the plasmid pBAC-SARS-Rep-RLuc was transfected into HEK293 cells at increasing concentrations of a p53-expressing plasmid. p53 strongly reduced replication of the SARS-CoV replicon by 65%, whereas it had no effect on the pcDNA3.0 Renilla luciferase (pcDNA3.0 RLuc) control (Fig. S6). The results demonstrate that p53 is a negative regulator of SARS-CoV replication.

MERS-CoV PL^{pro} and HCoV-NL63 PLP1/2 Interact with and Stabilize RCHY1 and Cause Endogenous p53 Degradation. As its name implies, the SUD is unique for the SARS-CoV, whereas PL^{pro} domains are relatively well-conserved in coronaviruses (39). Among the human coronaviruses, only SARS-CoV and MERS-CoV have one PL^{pro} domain, whereas most other HCoVs have two PL^{pro} domains, PLP1 and PLP2 (39, 45, 46). To investigate whether other HCoV PL^{pro}s also target RCHY1, similarly to what the SARS-CoV PL^{pro} does, we cloned the MERS-CoV PL^{pro} and the HCoV-NL63 PLP1/2 to perform a coIP RCHY1-binding assay. As a result, MERS-CoV PL^{pro} and NL63 PLP1 showed clear interaction with RCHY1 (Fig. 7*A*, compare lanes 2 and 3 with lane 1).

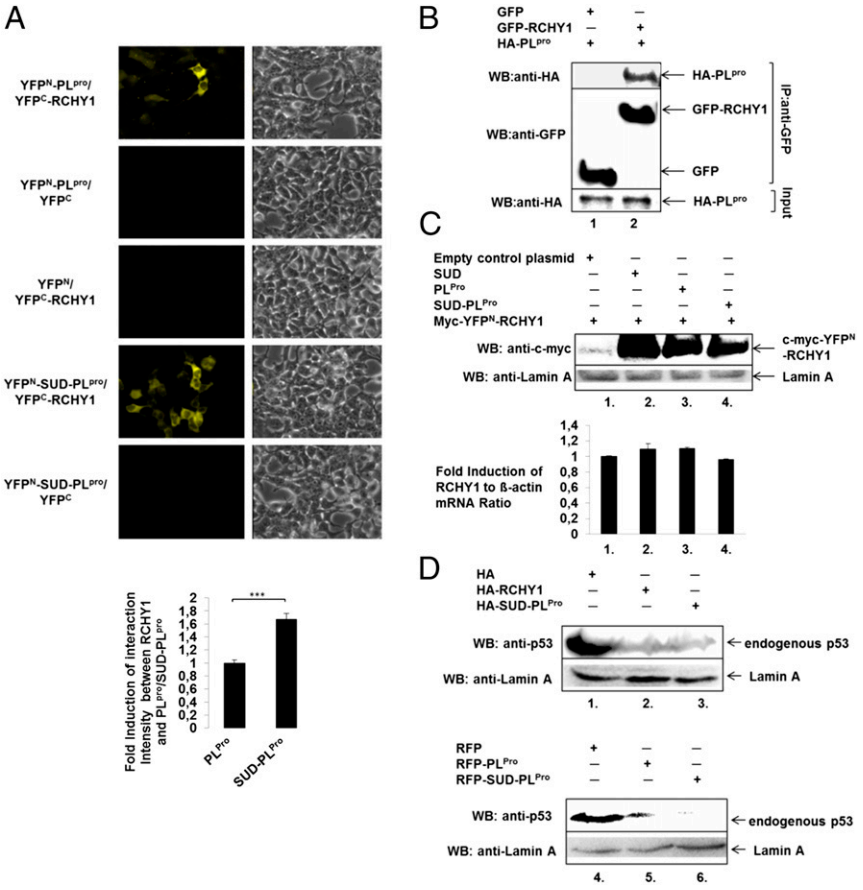

Fig. 5. SARS PL^{pro} interacts with RCHY1 and leads to accumulation of RCHY1 as well as p53 degradation. (*A*) YFP^N and YFP^C were fused to the N terminus of SARS PL^{pro} and to the N terminus of RCHY1, respectively. At 24 h after transfection, HEK293 cells were fixed with PFA and stained with DAPI. Samples were inspected with a fluorescent microscope (Leica DM4000 B, 40× objective; *Upper*). Pictures for statistical analysis were taken from at least five randomly chosen areas. Intensities of split-YFP and DAPI signals were measured with ImageJ software (***$P < 0.001$; *Lower*). (*B*) Plasmids expressing HA-tagged SARS PL^{pro} and GFP or GFP–RCHY1 fusion were transfected into HEK293 cells grown in 10-cm culture dishes. The coIP assay was performed as described before. (*C*) WB (*Upper*) Plasmids ectopically expressing SUD, PL^{pro}, or SUD–PL^{pro} fusion were transfected into HEK293 cells grown in a six-well plate. Cell lysates were prepared 24 h posttransfection and subjected to Western blotting with anti-Myc and anti-lamin A antibodies. qPCR: (*Lower*) Plasmids ectopically expressing SUD, PL^{pro}, or SUD–PL^{pro} fusion were transfected into HEK293 cells grown in a 24-well plate. At 24 h posttransfection, cells were harvested for total RNA extraction, first cDNA synthesis, and subsequent SYBR Green qPCR. The experiment was carried out in quadruplicates. (*D*) Indicated plasmids were transfected into HEK293 cells grown in a six-well plate. At 24 h posttransfection, cells were lysed for Western blotting with anti-p53 and anti-lamin A antibodies.

Most of the GFP-NL63 PLP2 was degraded with only a little intact protein remaining (Fig. 7*A*, lane 4). Nevertheless, a small amount of HA-RCHY1 could be coimmunoprecipitated by GFP-NL63 PLP2 (Fig. 7*A*, compare lane 4 with lane 1), implying interaction between these proteins. To further confirm the interaction, a split-YFP assay was performed (Fig. S7). Both MERS-CoV PL^{pro} and NL63 PLP2 showed clear interaction with RCHY1 in the nucleus and the cytosol, whereas NL63 PLP1 interacted with RCHY1 at the enodplasmic reticulum (ER).

Subsequently, we examined whether MERS-CoV PL^{pro} and NL63 PLP1/2 also stabilize RCHY1. As shown in Fig. 7*B*, all of the tested PL^{pro}s stimulated RCHY1 accumulation (compare lanes 2, 3, and 4 with lane 1). Indeed, the stabilization of RCHY1 by the NL63 PLP2 was dramatic (Fig. 7*B*, compare lane 4 with lane 1). Consistent with this result, all of the tested PL^{pro}s led to degradation of endogenous p53 as well (Fig. 7*C*). Thus, similarly to SARS-CoV PL^{pro}, MERS-CoV PL^{pro} and NL63 PLP1/2 also targeted RCHY1 for p53 degradation.

To find out whether p53 inhibits viral replication of other HCoVs in addition to SARS-CoV, the influence of p53 on NL63 replication was tested. Due to an extremely low transfection efficiency of p53 into the NL63-infected host Caco2 cells, HEK293 cells transiently expressing the NL63 receptor ACE2 were used as a substitute for Caco2. Real-time quantitative PCR (q-PCR) analysis revealed that NL63 replication was reduced by ∼30% in cells overexpressing p53, compared with control (Fig. 7*D*); this implies that p53 is an inhibitory factor not only for SARS-CoV but also for other HCoVs.

Discussion

PLP1/2 of the alphacoronavirus NL63 as well as the PL^{pro}s of SARS-CoV and MERS-CoV from the genus betacoronavirus physically interact with and stabilize RCHY1, and lead to p53 degradation. Because PL^{pro}s and PLPs are relatively well conserved among coronaviruses, it is highly likely that all of the coronaviruses share this strategy to antagonize the antiviral host factor p53. SUD alone strongly binds to and stabilizes RCHY1, leading to stimulation of p53 ubiquitination and degradation. The SUD–PL^{pro} fusion interacts with RCHY1 more intensively and causes stronger endogenous p53 degradation than SARS-CoV PL^{pro} alone. Hence, SUD functions as an enhancer for SARS-CoV Nsp3 to counteract p53, and this might contribute to the high virulence of SARS-CoV.

The mechanism of how SUD and PL^{pro}/PLPs stimulate the accumulation of RCHY1 remains unclear. It is known that phosphorylation by CAMKII or CDK9 leads to polyubiquitination and subsequent degradation of RCHY1 (14, 24), but SUD does not impair the phosphorylation activity of CAMK2D toward RCHY1. Because papain-like proteases of SARS-CoV, MERS-CoV, and NL63 possess deubiquitinating activity (39, 46, 47) and can stabilize RCHY1, we originally hypothesized that the latter may be a possible substrate for these enzymes. However, an in vitro deubiquitination assay has shown that SARS-CoV PL^{pro} does not deubiquitinate RCHY1. Thus, SUD and PL^{pro} should stabilize RCHY1 through other mechanisms, e.g., by counteracting the binding of RCHY1 to CDK9 or interfering with the homodimerization of RCHY1 for self-ubiquitination. Because both SUD and PL^{pro} physically interact with RCHY1, their mechanisms of RCHY1 stabilization might also be different from one another.

The protein level of RCHY1 is dramatically increased in the presence of SUD. As a result, RCHY1-mediated ubiquitination of p53 is enhanced and p53 degradation is stimulated. However, enhanced p53 degradation should not be the only consequence of RCHY1 accumulation. Besides p53, the substrate targets of the E3 ubiquitin ligase RCHY1 include transcription factors p63, p73, and c-Myc; checkpoint kinase Chk2; DNA polymerase polH; histone deacetylase HDAC1; and CDK inhibitor p27Kip1 (9, 10, 48–52). It can be hypothesized that during HCoV infection, the protein levels of various genes might also be down-regulated. SUD also physically

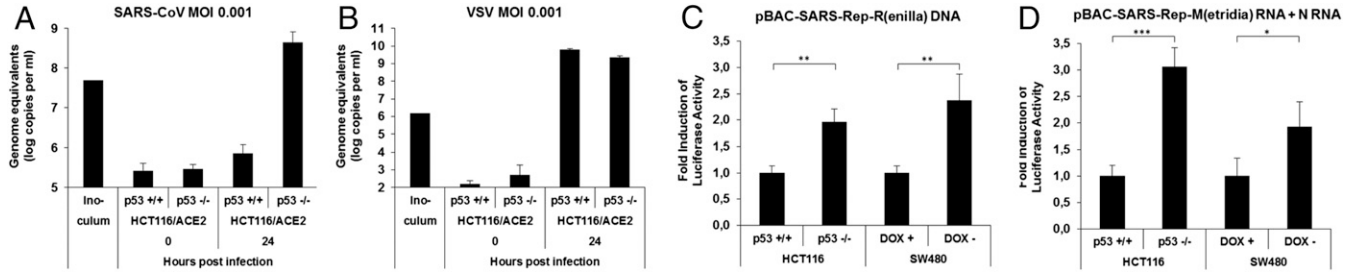

Fig. 6. p53 inhibits replication of a SARS-CoV. (*A* and *B*) Increased SARS-CoV growth in $p53^{-/-}$ ACE2-transgenic HCT116 cells. HCT116/ACE2 with p53 ($^{+/+}$) and without p53 ($^{-/-}$) were seeded at 2×10^5 cells per mL. After 24 h, cells were infected in quadruplicate with SARS-CoV (Frankfurt) and VSV (Indiana) at an MOI of 0.001. After 1 h at 37 °C, cells were washed with PBS and McCoy culture medium was replenished. Samples were taken at 0 and 24 h postinfection. Viral RNA was extracted by a Macherey-Nagel viral RNA kit. Real-time PCR was performed using virus-specific probes and primers with the One-Step SuperScript III Kit (Life Technologies) according to previous protocols. (*C* and *D*) HCT116 wild-type ($p53^{+/+}$) and knockout cells ($p53^{-/-}$) were transfected with HCoV SARS DNA and RNA replicons. p53 expression in SW480 cells was induced by adding 100 ng/mL DOX (DOX+) 24 h before transfection. SW480 cells without DOX induction (DOX–) were applied as control. pBAC-SARS-Rep-R(enilla)Luc DNA was transfected into cells using Lipofectamine 3000, and Renilla luciferase activity was measured from cell lysates after 24 h. The pBAC-SARS-Rep-M(etridia)Luc RNA was cotransfected with N-RNA by electroporation of cells, and Metridian luciferase activity was determined from medium supernatant after 20 h (*$P < 0.05$, **$P < 0.01$, ***$P < 0.001$).

interacts with CAMK2D, although it does not disturb phosphorylation of RCHY1 by CAMK2D. However, RCHY1 is neither the only substrate nor the only interacting partner of CAMK2D. The association of SUD and CAMK2D might alter the affinity of CAMK2D for other proteins, e.g., for its candidate binding partner IFN-γ receptor 2 (IFNGR2), which was discovered by Y2H screen (53). Alternatively, the interaction between SUD and CAMK2D might interfere with phosphorylation of STAT1 by CAMK2D, which is required for maximum IFN-γ–stimulated gene (ISG) expression (54). In addition to stimulation of p53 degradation, SUD probably features even more complex interferences with host cellular signaling pathways.

To date, p53 was found to serve as an antiviral factor against diverse positive-sense single-stranded RNA (ssRNA) viruses such as hepatitis C virus (HCV) and poliovirus; negative-sense ssRNA viruses such as influenza A virus; and the retrovirus HIV-1 (29, 31, 55, 56). p53 antiviral activity on Sendai virus replication was reported in the context of deubiquitination of MDM2 by coronaviral PL^{pro} and ubiquitination of p53 by MDM2 (30). In this mainly biochemical study, the inhibitory effect of p53 was not tested for coronaviruses. The authors had hypothesized regulatory influence of HCoV-NL63 PLP2 on the stability of MDM2, due (*i*) to structural similarities of PLP2, PL^{pro}, and the cellular deubiquitinase HAUSP, and (*ii*) to the preferential deubiquitination of MDM2 by HAUSP. Indeed, interaction of PLP2 and MDM2, deubiquitination of MDM2 by PLP2, and ubiquitination of p53 leading to proteasomal degradation was demonstrated.

Applying unbiased protein–protein interaction Y2H screens (34), we identified interaction of SUD with the cellular ubiquitin ligase RCHY1, which exerts similar ubiquitination activities on p53 as MDM2. We directly demonstrate, to our knowledge for the first time, that p53 inhibits replication of coronaviruses and provide evidence that SUD and PL^{pro}/PLPs antagonize the host defense factor p53 via stabilizing the E3 ubiquitin ligase RCHY1. So far, we have no hints on a conceivable involvement of MDM2, though it may well be that CoVs have developed different ways to down-regulate p53.

In addition, the deISGylating activity, exhibited by PL^{pro} domains, might further interfere with the ISGylation status of host proteins (57, 58). Decreased ISGylation of host proteins seems to positively mediate virus infection. It has been demonstrated that cellular ISGylation contributes to inhibition of replication of murine hepatitis virus strain 3 (59). Thus, CoV Nsp3 proteins containing SUD PL^{pro}/PLPs counteract the host defense in two distinct manners—one is p53 independent: the PL^{pro}/PLPs within Nsp3 exert a direct deISGylation activity to interfere with cellular ISGylation; the other is p53 dependent: Nsp3 proteins lead to p53 degradation by stabilizing RCHY1. These results may open new possibilities to therapeutically target SARS infections in the future.

Materials and Methods

Plasmid Constructs. The fragments c-Myc-YFP^N (amino acids 1–155) and HA-YFP^C (amino acids 156–239) were amplified with designed primers (Table S1) from the template plasmids pSPYNE-35S and pSPYCE-35S (37), respectively. The obtained PCR fragments were subsequently cloned into the pTREX-dest30-PrA Gateway-compatible vector via AgeI/XhoI cleavage sites or into the pTREX-dest30-ct-PrA Gateway-compatible vector (60) via SpeI/ApaI sites to replace the protein A tag, yielding pDEST-c-Myc-YFP^N (c-Myc-YFP^N fused to N terminus of a test gene) and pDEST-HA-YFP^c (HA-YFP^C fused to N terminus of a test gene) or pDEST-ct-c-Myc-YFP^N (c-Myc-YFP^N fused to C terminus of a test gene) and pDEST-ct-HA-YFP^c (HA-YFP^C fused to C terminus of a test gene) split-YFP vectors. SUD, RCHY1, MERS-CoV MC, SARS-CoV PL^{pro}, MERS-CoV PL^{pro}, NL63 PLP1/2, and the truncated fragments of SUD and RCHY1 amplified with corresponding primers (Table S1) were first BP Gateway-cloned into the pDONR207 vector and consequently LR Gateway-cloned into the pDEST-c-Myc-YFP^N, pDEST-HA-YFP^c, pDEST-ct-c-Myc-YFP^N, pDEST-ct-HA-YFP^c vectors, yielding constructs for split-YFP assays. CAMK2D and p53 were selected from a human cDNA library of 5,000 different, individually cloned genes in pDONR223 vectors, as described before (34). CAMK2D and p53 were then cloned from pDONR223 to split-YFP vectors via the LR reaction.

To generate RFP- or GFP-tagged constructs, the RFP and GFP fragments without NLS (nuclear localization signal) were amplified with designed primers (Table S1) from the template plasmids pNLS-TagRFP and pNLS-TagGFP, respectively (61). The PCR products were subsequently cloned into pTREX-dest30-PrA via AgeI/XhoI sites or into pTREX-dest30-ct-PrA via SpeI/ApaI sites to replace the protein A tag, yielding pDEST-RFP and pDEST-GFP or pDEST-ct-RFP and pDEST-ct-GFP Gateway-compatible destination vectors. RCHY1, SUD, SARS-CoV PL^{pro}, SUD–PL^{pro} fusion, MERS-CoV PL^{pro}, NL63 PLP1/2, and p53 were subsequently cloned into the obtained RFP- and GFP-tagged destination vectors via the LR reaction. CDK9 was selected from the human cDNA library described above and, finally, LR Gateway-cloned into the pDEST-ct-GFP vector, yielding the CDK9–GFP fusion construct. The pDEST-C-tag-HA and pDEST-N-tag-HA Gateway-compatible destination vectors were used to generate HA-tagged fusions. Ubiquitin was amplified with designed primers (Table S1) from the synthesized first cDNA of HEK293 cells and cloned into the pDONR207 vector via the BP reaction. Calmodulin was selected from the human cDNA library as described above. Ubiquitin, calmodulin, CAMK2D, RCHY1, SUD–PL^{pro}, and SARS-CoV PL^{pro} were finally cloned into pDEST-HA or pDEST-ct-HA vectors via the LR reaction.

Cell Cultures and Transfection. HEK293 and HCT116 $p53^{+/+}$/$p53^{-/-}$ cells were cultured at standard conditions (*SI Materials and Methods*). For introduction of the ACE2 receptor into HCT116 $p53^{+/+}$ and $p53^{-/-}$, cells 2×10^5 cells/mL were transduced with human ACE2-carrying lentiviruses at an MOI of 0.005. Lentiviruses were provided in McCoy's 5A supplemented with polybrene (1 μg/mL). After 48 h, the supernatant was removed, cells were washed with PBS, and McCoy's 5A containing 1 μg/mL puromycin was added for selection. Selective medium was changed every 3 d. After 10 d, surviving cells were expanded and tested for hACE2 protein expression by immunofluorescence assay and Western blot analysis as described previously (62).

Split-YFP. Fluorescence microscopy was performed according to standard procedures and is described in detail in *SI Materials and Methods*.

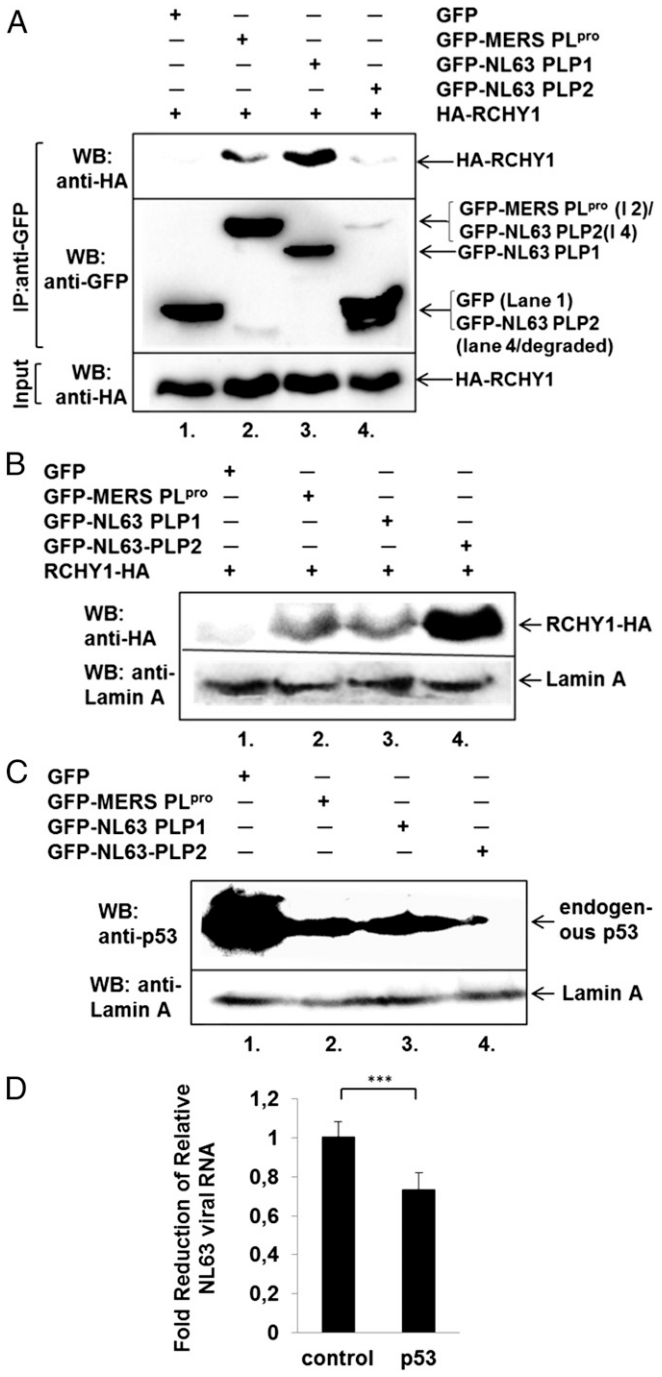

Fig. 7. MERS PL^{pro} and NL63 PLP1/2 lead to accumulation of RCHY1 and p53 degradation. (*A*) The indicated plasmids were transfected to HEK293 cells growing in 10-cm culture dishes. CoIP was performed as described before. (*B*) The indicated plasmids were transfected to HEK293 cells growing in a six-well plate. At 24 h posttransfection, cells were lysed. The lysates were Western blotted with anti-HA and anti-lamin A antibodies. (*C*) At 24 h after transfection with the indicated plasmids into HEK293, cells were harvested and Western blotted with anti-p53 and anti-lamin A antibodies. (*D*) HEK293 cells were cotransfected with plasmids overexpressing RFP-ACE2 and plasmids overexpressing GFP control or p53-GFP. At 24 h after transfection, cells were inoculated with NL63 viruses of MOI 0.4 at 37 °C for 1 h. At 24 h after infection with NL63 virus, total RNA was extracted from cell lysates. Viral RNA was analyzed by qPCR with NL63-specific primers and standardized with RFP-ACE2 intensity. Experiments were performed in sextuplicates. ***$P < 0.001$.

CoIP and Western Blot. GFP fusions and complexed proteins were immunoprecipitated by GFP-Trap_A beads (ChromoTek) according to manufacturer's protocol under native conditions (*SI Materials and Methods*). Detailed Western blot protocols were described elsewhere (63).

qPCR. Quantification NL63 viral RNA (63) and of cellular mRNAs is described in detail in *SI Materials and Methods*.

In Vivo Ubiquitination Assay. Plasmids expressing HA-tagged ubiquitin, c-Myc-YFP^N-tagged RCHY1 (c-Myc-YFP^N-RCHY1), substrate protein (GFP control or p53-GFP), and effector protein (RFP control, SUD–RFP fusion, RFP-SUD–PL^{pro} fusion, or RFP–PL^{pro} fusion) were cotransfected into HEK293 cells using the polyethylenimine (PEI) method. At 24 h posttransfection, cells were lysed with lysis buffer containing 10 mM Tris·HCl (pH 7.5), 150 mM NaCl, 0.5 mM EDTA, 0.5% Nonidet P-40, 10 mM N-ethylmaleimide, and protease inhibitor (Complete ULTRA Tablets; Roche). Subsequently, GFP-Trap_A beads (ChromoTek) were used to purify GFP and p53-GFP from the cell lysates. The purified GFP and p53-GFP were examined with anti-HA and anti-GFP (ChromoTek) antibodies by Western blot for the test of in vivo ubiquitination of p53.

In Vitro Deubiquitination Assay. HEK293 cells growing on 10-cm dishes were cotransfected with GFP-RCHY1, HA-ubiquitin, calmodulin1-RFP, and CAMK2D-c-Myc-YFP^N. At 23 h posttransfection, cells were treated with PMA to a final concentration of 20 ng/mL and ionomycin to a final concentration of 1 μM to activate CAMK2D. At 90 min after the treatment, cells were harvested and GFP-RCHY1 protein was purified with GFP-trap_A beads (ChromoTek). The purified bead-bound GFP-RCHY1 was subsequently incubated with 10 μM SARS-CoV PL^{pro} protein at 25 °C for 30 min in a buffer containing 10 mM Tris·HCl (pH 7.5), 150 mM NaCl, 0.5 mM EDTA, and 2 μM DTT. After incubation, the beads were washed twice with washing buffer containing 10 mM Tris·HCl (pH 7.5), 150 mM NaCl, and 0.5 mM EDTA. The bead-bound GFP-RCHY1 was finally examined with anti-HA and anti-GFP (ChromoTek) antibodies by Western blot.

Purification of Recombinant SARS-CoV PL^{pro}. The PL^{pro} of SARS-CoV (strain TOR2; GenBank accession no. AY274119) is part of Nsp3 and comprises 319 aa residues, corresponding to Glu1541–Tyr1859 of pp1a. A gene coding for the PL^{pro} was amplified by the PCR using the forward primer 5′-CTAGCTAGCGAGGTTAAGACTATAAAAGTGTTC-3′ and the reverse primer 5′-CCGCTCGAGTTAATACGACACAGGCTTGATGGTTGTAG-3′. The resulting PCR product was digested with restriction enzymes NheI and XhoI for ligation into pET-28a (Novagen). Cloning was designed to include an N-terminal hexahistidine (His_6) tag and a thrombin cleavage site. The recombinant plasmid was verified by DNA sequencing. Expression of the PL^{pro} gene and purification of the protein were carried out by a method described previously (64).

In Vivo Kinase Activity Assay. Plasmids expressing calmodulin-HA, CAMK2D-c-Myc-YFP^N, substrate protein (GFP control or GFP–RCHY1), and effector protein (RFP control or SUD–RFP fusion) were cotransfected into HEK293 cells using the PEI method. Medium was changed 20 h posttransfection. Then the cells were treated with PMA to a final concentration of 20 ng/mL and ionomycin to a final concentration of 1 μM. Two hours after the treatment, cells were harvested and GFP-trap_A beads (ChromoTek) were used to purify GFP and the GFP–RCHY1 fusion from the cell lysates. Purified GFP and GFP–RCHY1 fusion proteins were subsequently examined with anti–phospho-Ser/Thr (QIAGEN) and anti-GFP (ChromoTek) antibodies by Western blot for in vivo phosphorylation.

Luciferase Activity Assay. Transfected cells were harvested with Renilla Luciferase Assay System Kit (Promega). The luciferase activity was then measured with a FLUOstar OPTIMA fluorescence plate reader (BMG LABTECH).

Statistical Analysis. qPCR and luciferase measurement data are shown as mean ± SD of tri- or quadruplicated values and analyzed by one-way or two-way ANOVA with Bonferroni´s posttest (or by *t* test) using Prism 5 (GraphPad Software Inc.). *P* values of 0.05 or less were considered significant.

Virus Infection Experiments. Cell cultures were infected in quadruplicate with either SARS-CoV (strain Frankfurt) und VSV (strain Indiana) at a multiplicity of infection of 0.001. After virus adsorption, cells were washed with PBS and cell culture medium was replenished. Samples were taken at 0 and 24 h postinfection. Viral RNA was extracted by a Macherey-Nagel viral RNA kit. Real-time PCR was performed using virus-specific probes and primers with the One-Step SuperScript III kit (Life Technologies) according to previous protocols (34).

ACKNOWLEDGMENTS. HCT 116 cell lines and derivatives were kindly provided by Bert Vogelstein (Johns Hopkins Medical School). This work was supported by the Bundesministerium für Bildung und Forschung of the German Government,

Zoonosis Network, Consortium on Ecology and Pathogenesis of SARS Project Code 01KI1005A,F (to A.v.B.); German Center for Infection Research (partner sites Munich) Project Code 8025801803 (to A.v.B.); and Lübeck Project Code 8000 204-3 (to R.H.).

1. Stadler K, et al. (2003) SARS–beginning to understand a new virus. *Nat Rev Microbiol* 1(3):209–218.
2. Hilgenfeld R, Peiris M (2013) From SARS to MERS: 10 years of research on highly pathogenic human coronaviruses. *Antiviral Res* 100(1):286–295.
3. Graham RL, Donaldson EF, Baric RS (2013) A decade after SARS: Strategies for controlling emerging coronaviruses. *Nat Rev Microbiol* 11(12):836–848.
4. Ma-Lauer Y, Lei J, Hilgenfeld R, von Brunn A (2012) Virus-host interactomes–antiviral drug discovery. *Curr Opin Virol* 2(5):614–621.
5. Báez-Santos YM, St John SE, Mesecar AD (2015) The SARS-coronavirus papain-like protease: Structure, function and inhibition by designed antiviral compounds. *Antiviral Res* 115:21–38.
6. Tan J, et al. (2009) The SARS-unique domain (SUD) of SARS coronavirus contains two macrodomains that bind G-quadruplexes. *PLoS Pathog* 5(5):e1000428.
7. Kusov Y, Tan J, Alvarez E, Enjuanes L, Hilgenfeld R (2015) A G-quadruplex-binding macrodomain within the "SARS-unique domain" is essential for the activity of the SARS-coronavirus replication-transcription complex. *Virology* 484:313–322.
8. Leng RP, et al. (2003) Pirh2, a p53-induced ubiquitin-protein ligase, promotes p53 degradation. *Cell* 112(6):779–791.
9. Jung YS, Qian Y, Chen X (2011) The p73 tumor suppressor is targeted by Pirh2 RING finger E3 ubiquitin ligase for the proteasome-dependent degradation. *J Biol Chem* 286(41):35388–35395.
10. Jung YS, Qian Y, Yan W, Chen X (2013) Pirh2 E3 ubiquitin ligase modulates keratinocyte differentiation through p63. *J Invest Dermatol* 133(5):1178–1187.
11. Halaby MJ, Hakem R, Hakem A (2013) Pirh2: An E3 ligase with central roles in the regulation of cell cycle, DNA damage response, and differentiation. *Cell Cycle* 12(17): 2733–2737.
12. Abou Zeinab R, Wu H, Sergi C, Leng RP (2013) Residues 240-250 in the C-terminus of the Pirh2 protein complement the function of the RING domain in self-ubiquitination of the Pirh2 protein. *PLoS One* 8(12):e82803.
13. Chen M, et al. (2005) Inhibition of ubiquitination and stabilization of human ubiquitin E3 ligase PIRH2 by measles virus phosphoprotein. *J Virol* 79(18):11824–11836.
14. Duan S, et al. (2007) Phosphorylation of Pirh2 by calmodulin-dependent kinase II impairs its ability to ubiquitinate p53. *EMBO J* 26(13):3062–3074.
15. Hook SS, Means AR (2001) Ca(2+)/CaM-dependent kinases: From activation to function. *Annu Rev Pharmacol Toxicol* 41:471–505.
16. Hoelz A, Nairn AC, Kuriyan J (2003) Crystal structure of a tetradecameric assembly of the association domain of Ca2+/calmodulin-dependent kinase II. *Mol Cell* 11(5):1241–1251.
17. Colbran RJ (2004) Targeting of calcium/calmodulin-dependent protein kinase II. *Biochem J* 378(Pt 1):1–16.
18. Bieging KT, Mello SS, Attardi LD (2014) Unravelling mechanisms of p53-mediated tumour suppression. *Nat Rev Cancer* 14(5):359–370.
19. Hünten S, et al. (2015) p53-regulated networks of protein, mRNA, miRNA, and lncRNA expression revealed by integrated pulsed stable isotope labeling with amino acids in cell culture (pSILAC) and next generation sequencing (NGS) analyses. *Mol Cell Proteomics* 14(10):2609–2629.
20. Haupt Y, Maya R, Kazaz A, Oren M (1997) Mdm2 promotes the rapid degradation of p53. *Nature* 387(6630):296–299.
21. Honda R, Tanaka H, Yasuda H (1997) Oncoprotein MDM2 is a ubiquitin ligase E3 for tumor suppressor p53. *FEBS Lett* 420(1):25–27.
22. Shloush J, et al. (2011) Structural and functional comparison of the RING domains of two p53 E3 ligases, Mdm2 and Pirh2. *J Biol Chem* 286(6):4796–4808.
23. Li M, et al. (2003) Mono- versus polyubiquitination: Differential control of p53 fate by Mdm2. *Science* 302(5652):1972–1975.
24. Bagashev A, et al. (2013) Cdk9 phosphorylates Pirh2 protein and prevents degradation of p53 protein. *Cell Cycle* 12(10):1569–1577.
25. Maya R, et al. (2001) ATM-dependent phosphorylation of Mdm2 on serine 395: role in p53 activation by DNA damage. *Genes Dev* 15(9):1067–1077.
26. Claudio PP, et al. (2006) Cdk9 phosphorylates p53 on serine 392 independently of CKII. *J Cell Physiol* 208(3):602–612.
27. Sato Y, Tsurumi T (2013) Genome guardian p53 and viral infections. *Rev Med Virol* 23(4):213–220.
28. Vogelstein B, Lane D, Levine AJ (2000) Surfing the p53 network. *Nature* 408(6810):307–310.
29. Mukerjee R, Claudio PP, Chang JR, Del Valle L, Sawaya BE (2010) Transcriptional regulation of HIV-1 gene expression by p53. *Cell Cycle* 9(22):4569–4578.
30. Yuan L, et al. (2015) p53 degradation by a coronavirus papain-like protease suppresses type I interferon signaling. *J Biol Chem* 290(5):3172–3182.
31. Muñoz-Fontela C, et al. (2011) p53 serves as a host antiviral factor that enhances innate and adaptive immune responses to influenza A virus. *J Immunol* 187(12):6428–6436.
32. Saha A, et al. (2009) Epstein-Barr virus nuclear antigen 3C augments Mdm2-mediated p53 ubiquitination and degradation by deubiquitinating Mdm2. *J Virol* 83(9):4652–4669.
33. Sato Y, et al. (2009) Degradation of phosphorylated p53 by viral protein-ECS E3 ligase complex. *PLoS Pathog* 5(7):e1000530.
34. Pfefferle S, et al. (2011) The SARS-coronavirus-host interactome: Identification of cyclophilins as target for pan-coronavirus inhibitors. *PLoS Pathog* 7(10):e1002331.
35. Hubner NC, et al. (2010) Quantitative proteomics combined with BAC TransgeneOmics reveals in vivo protein interactions. *J Cell Biol* 189(4):739–754.
36. Keilhauer EC, Hein MY, Mann M (2015) Accurate protein complex retrieval by affinity enrichment mass spectrometry (AE-MS) rather than affinity purification mass spectrometry (AP-MS). *Mol Cell Proteomics* 14(1):120–135.
37. Walter M, et al. (2004) Visualization of protein interactions in living plant cells using bimolecular fluorescence complementation. *Plant J* 40(3):428–438.
38. Johnson MA, Chatterjee A, Neuman BW, Wüthrich K (2010) SARS coronavirus unique domain: Three-domain molecular architecture in solution and RNA binding. *J Mol Biol* 400(4):724–742.
39. Barretto N, et al. (2005) The papain-like protease of severe acute respiratory syndrome coronavirus has deubiquitinating activity. *J Virol* 79(24):15189–15198.
40. Lindner HA, et al. (2005) The papain-like protease from the severe acute respiratory syndrome coronavirus is a deubiquitinating enzyme. *J Virol* 79(24):15199–15208.
41. Lee JT, Gu W (2010) The multiple levels of regulation by p53 ubiquitination. *Cell Death Differ* 17(1):86–92.
42. Duan L, et al. (1994) The tumor suppressor protein p53 strongly alters human immunodeficiency virus type 1 replication. *J Virol* 68(7):4302–4313.
43. Brown C, Kowalczyk AM, Taylor ER, Morgan IM, Gaston K (2008) P53 represses human papillomavirus type 16 DNA replication via the viral E2 protein. *Virol J* 5:5.
44. Bunz F, et al. (1998) Requirement for p53 and p21 to sustain G2 arrest after DNA damage. *Science* 282(5393):1497–1501.
45. Bailey-Elkin BA, et al. (2014) Crystal structure of the Middle East respiratory syndrome coronavirus (MERS-CoV) papain-like protease bound to ubiquitin facilitates targeted disruption of deubiquitinating activity to demonstrate its role in innate immune suppression. *J Biol Chem* 289(50):34667–34682.
46. Clementz MA, et al. (2010) Deubiquitinating and interferon antagonism activities of coronavirus papain-like proteases. *J Virol* 84(9):4619–4629.
47. Mielech AM, Kilianski A, Baez-Santos YM, Mesecar AD, Baker SC (2014) MERS-CoV papain-like protease has delSGylating and deubiquitinating activities. *Virology* 450-451:64–70.
48. Hakem A, et al. (2011) Role of Pirh2 in mediating the regulation of p53 and c-Myc. *PLoS Genet* 7(11):e1002360.
49. Bohgaki M, et al. (2013) The E3 ligase PIRH2 polyubiquitylates CHK2 and regulates its turnover. *Cell Death Differ* 20(6):812–822.
50. Jung YS, Liu G, Chen X (2010) Pirh2 E3 ubiquitin ligase targets DNA polymerase eta for 20S proteasomal degradation. *Mol Cell Biol* 30(4):1041–1048.
51. Logan IR, et al. (2006) Human PIRH2 enhances androgen receptor signaling through inhibition of histone deacetylase 1 and is overexpressed in prostate cancer. *Mol Cell Biol* 26(17):6502–6510.
52. Hattori T, et al. (2007) Pirh2 promotes ubiquitin-dependent degradation of the cyclin-dependent kinase inhibitor p27Kip1. *Cancer Res* 67(22):10789–10795.
53. Wang J, et al. (2011) Toward an understanding of the protein interaction network of the human liver. *Mol Syst Biol* 7:536.
54. Nair JS, et al. (2002) Requirement of Ca2+ and CaMKII for Stat1 Ser-727 phosphorylation in response to IFN-gamma. *Proc Natl Acad Sci USA* 99(9):5971–5976.
55. Dharel N, et al. (2008) Potential contribution of tumor suppressor p53 in the host defense against hepatitis C virus. *Hepatology* 47(4):1136–1149.
56. Pampin M, Simonin Y, Blondel B, Percherancier Y, Chelbi-Alix MK (2006) Cross talk between PML and p53 during poliovirus infection: Implications for antiviral defense. *J Virol* 80(17):8582–8592.
57. Báez-Santos YM, Mielech AM, Deng X, Baker S, Mesecar AD (2014) Catalytic function and substrate specificity of the papain-like protease domain of nsp3 from the Middle East respiratory syndrome coronavirus. *J Virol* 88(21):12511–12527.
58. Ratia K, Kilianski A, Baez-Santos YM, Baker SC, Mesecar A (2014) Structural basis for the ubiquitin-linkage specificity and deISGylating activity of SARS-CoV papain-like protease. *PLoS Pathog* 10(5):e1004113.
59. Ma XZ, et al. (2014) Protein interferon-stimulated gene 15 conjugation delays but does not overcome coronavirus proliferation in a model of fulminant hepatitis. *J Virol* 88(11):6195–6204.
60. Katzen F (2007) Gateway® recombinational cloning: A biological operating system. *Expert Opin Drug Discov* 2(4):571–589.
61. Dambacher S, et al. (2012) CENP-C facilitates the recruitment of M18BP1 to centromeric chromatin. *Nucleus* 3(1):101–110.
62. Müller MA, et al. (2012) Human coronavirus EMC does not require the SARS-coronavirus receptor and maintains broad replicative capability in mammalian cell lines. *MBio* 3(6):e00515-12.
63. Carbajo-Lozoya J, et al. (2014) Human coronavirus NL63 replication is cyclophilin A-dependent and inhibited by non-immunosuppressive cyclosporine A-derivatives including Alisporivir. *Virus Res* 184:44–53.
64. Lei J, et al. (2014) Crystal structure of the papain-like protease of MERS coronavirus reveals unusual, potentially druggable active-site features. *Antiviral Res* 109:72–82.
65. Schneider CA, Rasband WS, Eliceiri KW (2012) NIH Image to ImageJ: 25 years of image analysis. *Nat Methods* 9(7):671–675.
66. Tsukamoto T, et al. (2000) Visualization of gene activity in living cells. *Nat Cell Biol* 2(12):871–878.
67. Herce HD, Deng W, Helma J, Leonhardt H, Cardoso MC (2013) Visualization and targeted disruption of protein interactions in living cells. *Nat Commun* 4:2660.
68. Rothbauer U, et al. (2006) Targeting and tracing antigens in live cells with fluorescent nanobodies. *Nat Methods* 3(11):887–889.
69. Jackstadt R, et al. (2013) AP4 is a mediator of epithelial-mesenchymal transition and metastasis in colorectal cancer. *J Exp Med* 210(7):1331–1350.
70. Siemens H, et al. (2011) miR-34 and SNAIL form a double-negative feedback loop to regulate epithelial-mesenchymal transitions. *Cell Cycle* 10(24):4256–4271.

Supporting Information

Ma-Lauer et al. 10.1073/pnas.1603435113

SI Materials and Methods

Cell Cultures and Transfection. HEK293 cells (ATCC CCL-81) were cultured in DMEM (Gibco) containing 10% (vol/vol) FBS and 1% penicillin/streptomycin in plates. Plasmids were transfected into cells using Lipofectamine 3000 Reagent (Invitrogen) or 25 kDa polyethylenimine (PEI) when the cells were 80% confluent. HCT116 $p53^{+/+}$ and $p53^{-/-}$ cells (obtained from Bert Vogelstein, Ludwig Center at Johns Hopkins, Howard Hughes Medical Institute, Baltimore) were cultured in McCoy's 5A Medium (Gibco) containing 10% (vol/vol) FBS and 1% penicillin/streptomycin. SW480 cells (ATCC CCL-228) were maintained in DMEM with 10% (vol/vol) FBS, 1% L-glutamine, 1% penicillin/streptomycin, and 4 μg/mL puromycin. HCT116 and SW480 cells were transfected with Lipofectamine 3000 Reagent (Invitrogen) or by electroporation (140 V, 25 ms).

Fluorescence-3-Hybrid. BHK cells containing a lac operator (*lac*O) array (65) were cultured in DMEM supplemented with 10% (vol/vol) FBS. The fluorescence-3-hybrid (F3H) assay was performed as previously described (67). In brief, BHK cells were seeded on glass coverslips and triple-transfected with plasmids encoding the fluorescent fusions and GBP–LacI (67, 68) using polyethylenimine (Sigma). After 48 h, cells were fixed with 3.7% (vol/vol) formaldehyde and stained with 200 ng/mL DAPI after permeabilization. Samples were mounted in VectaShield medium (Vector Laboratories) and sealed with fingernail polish.

Sample slides were analyzed using a laser scanning confocal microscope (TCS SP5; Leica) equipped with 63× oil-immersion N.A. 1.40 objective. DAPI, GFP, and RFP were excited with 405-, 488-, and 561-nm lasers, respectively. Signals were collected with photomultiplier tube detectors and recorded as TIFF files with a size of 512 × 512 pixels. Images were processed with ImageJ (version 1.48) and organized with Adobe Illustrator (CS 5.1) software.

Split-YFP and Fluorescence Microscopy. HEK293 cells were seeded directly on autoclaved coverslips and cultured in 24-well plates. Split-YFP plasmids were cotransfected to cells at 80% confluency using Lipofectamine 3000 (Invitrogen). At 24 h after transfection, cells on coverslips were directly examined under a microscope (Leica DM4000 B). Pictures were taken with a 40× objective.

For DAPI staining, cells were fixed with 2% (wt/vol) PFA in PBS at room temperature (RT) for 15 min. After PBS washes, the cells were permeabilized with 0.1% Triton in PBS at RT for 10 min and subsequently washed twice with PBS and stained with DAPI at RT in the dark for 10 min. Finally, the cells were washed three times with PBS and the coverslips were embedded on object slides with a drop of mounting medium. The samples were examined with a fluorescent microscope (Leica DM4000 B) through its 10× objective.

Coimmunoprecipitation and Western Blot. Plasmids were transfected into HEK293 cells grown in 10-cm culture dishes with PEI. At 24 h after transfection, cells were lysed with lysis buffer containing 10 mM Tris·HCl (pH 7.5), 150 mM NaCl, 0.5 mM EDTA, 0.5% Nonidet P-40, and protease inhibitor (Complete ULTRA Tablets; Roche). GFP-Trap_A beads for IP of GFP fusion proteins (ChromoTek) were used to pull down the GFP complex via its standard protocol under the native conditions. The eluted samples and cell lysates were then analyzed by Western blotting. The antibodies used for coIP and Western blotting were received from the following providers: anti-SARS-CoV nsp3 (ROCKLAND), anti-GFP (ChromoTek), anti-lamin A (BETHYL), anti-p53 (Santa Cruz), anti–phospho-Ser/Thr (QIAGEN), anti-Myc (Roche), and anti-HA (Roche).

qPCR. For measurement of the RCHY1 mRNA level, plasmids were transfected into HEK293 cells growing in a 24-well plate by using Lipofectamine 3000 (Invitrogen). At 24 h posttransfection, total RNA was extracted from the cells with a High Pure RNA Isolation Kit (Roche). The first cDNA strand was synthesized with the oligonucleotide $(dT)_{20}$ and SuperScript II RT (Invitrogen). Quantification was subsequently carried out by qPCR using RCHY1- and β-actin–specific primers (Table S1) and FastStart Essential DNA Green Master (Roche).

For analysis of NL63 viral RNA, plasmids expressing RFP-ACE2 and plasmids expressing GFP control or p53-GFP were cotransfected (Lipofectamine 3000; Invitrogen) into HEK293 cells growing in a 24-well plate. At 24 h after transfection, the medium was changed. Transfected cells were then inoculated with NL63 virus (MOI 0.4) at 37 °C for 1 h. Subsequently, cells were washed with PBS and cultured with fresh medium. At 24 h after infection, pictures of the cells were taken under a 10× objective of a fluorescence microscope (Leica DMI4000 B). The RFP-ACE2 intensity was then quantified using ImageJ software (66). Finally, total RNA was extracted from cell lysates with a High Pure RNA Isolation Kit (Roche) and processed with q-PCR (SensiFAST Probe Hi-ROX One-Step Kit; BIOLINE) using NL63-specific primers (63). The intensity of NL63 viral RNA was standardized with the intensity of RFP-ACE2 for calculation of data presented in Fig. 7*D*.

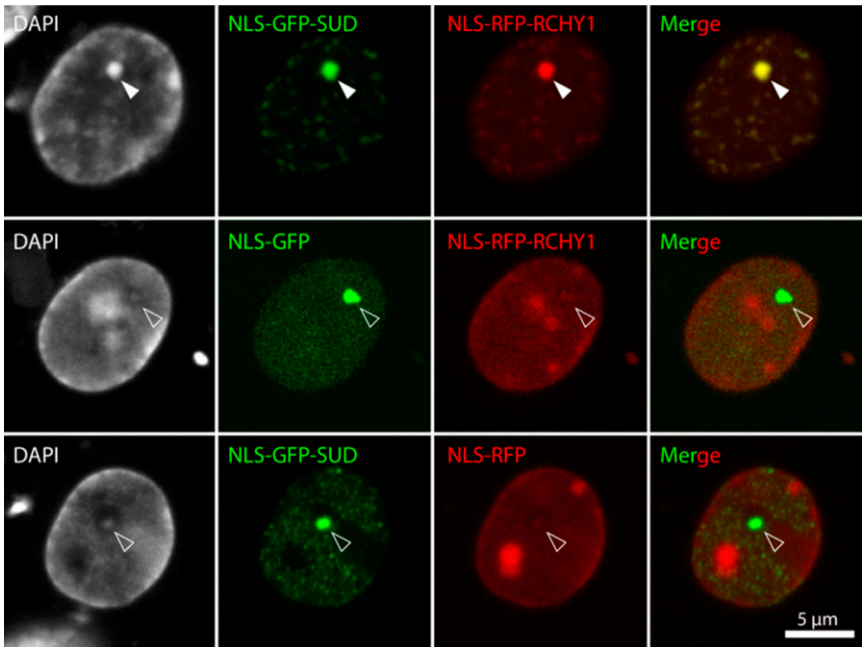

Fig. S1. SUD interacts with RCHY1 in F3H assay. SUD protein tagged with NLS-GFP are captured at the *lac*O array by the coexpressed GBP–LacI fusion and visualized as a green spot with fluorescence microscopy. The NLS-RFP–tagged RCHY1 protein colocalizes with the SUD protein at the *lac*O spot, indicating an interaction between these two proteins (*Top*, *lac*O spot is marked with filled arrowhead). In the absence of either SUD (*Middle*) or RCHY1 (*Bottom*), the RFP fusions are not recruited to the *lac*O spot (open arrowhead), demonstrating the specificity of this interaction assay. The nucleus was stained with DAPI. (Scale bar: 5 μm.)

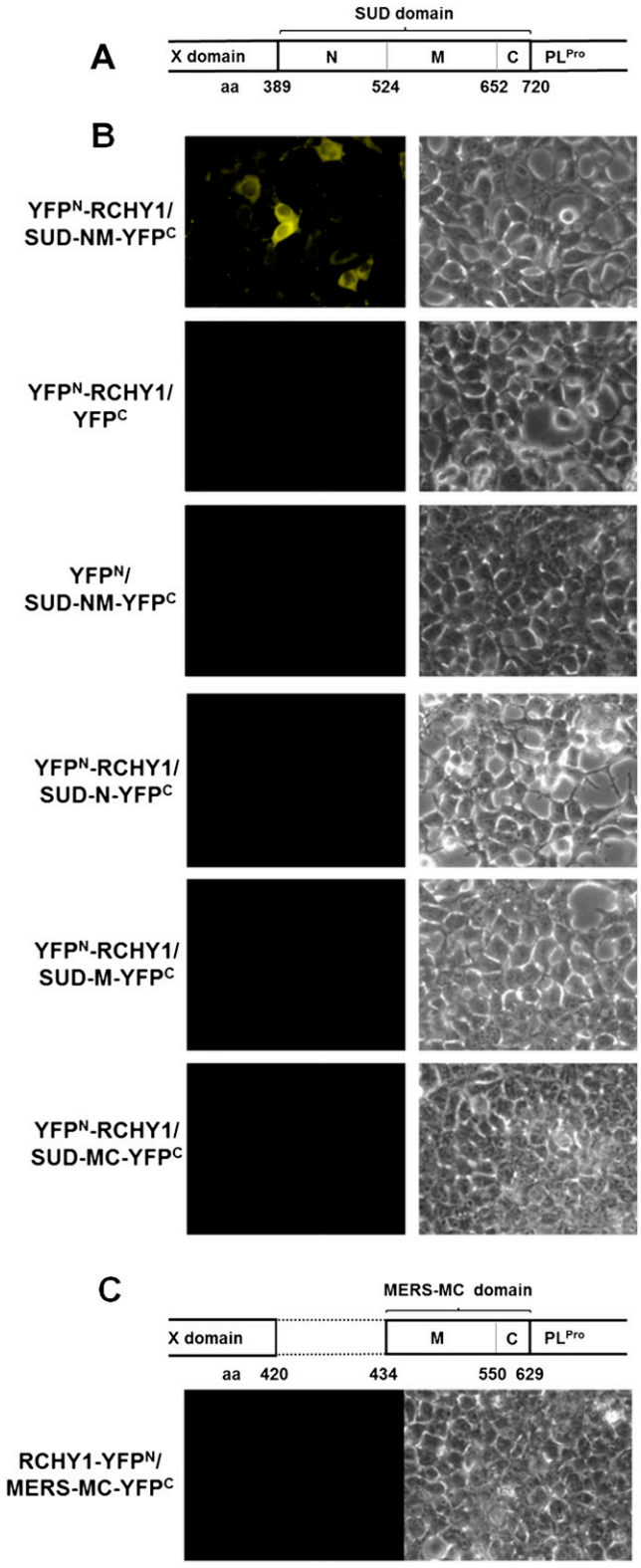

Fig. S2. SUD-NM interacts with RCHY1. At 24 h posttransfection of the expression plasmids into HEK293 cells, YFP signal was examined by fluorescence microscopy. (*A*) Scheme of SUD location within SARS nsp3, which consists of 1,922 amino acids. (*B*) YFP^N was fused to the N terminus of RCHY1, and YFP^C was fused to the C terminus of truncated SUD fragments. (*C*) YFP^N was fused to the C terminus of RCHY1, and YFP^C was fused to the C terminus of MERS-MC domain, i.e., SUD-like domain (schematically presented in *Upper*).

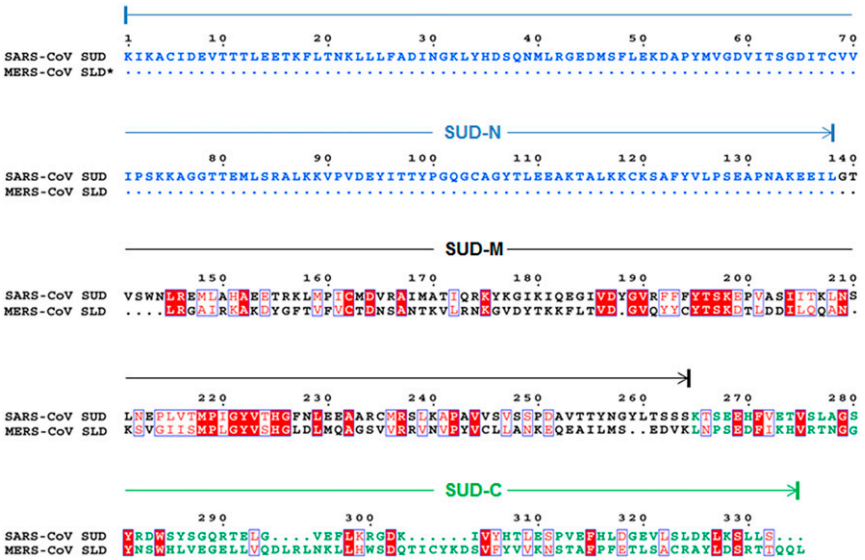

Fig. S3. Alignment of SUD with MERS homolog. The figure was created by using the program ESPript. SARS-CoV-SUD-N subdomain is indicated in blue; SARS-CoV-SUD-M subdomain and MERS-CoV-SUD-M homolog are indicated in black; SARS-CoV-SUD-C subdomain and MERS-CoV-SUD-C homolog are indicated in green. SLD, SUD-like domain.

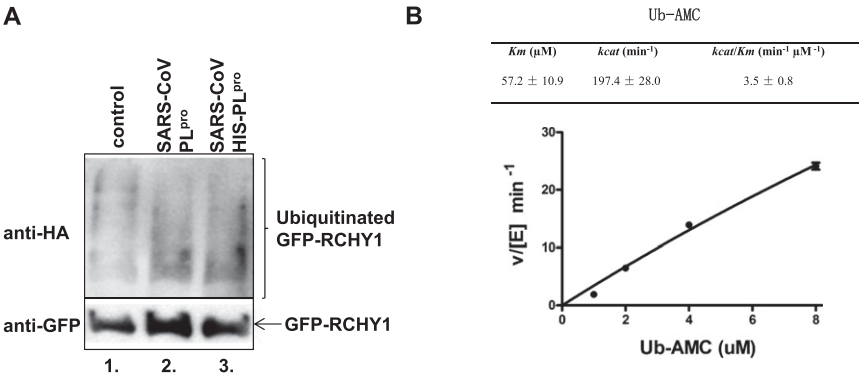

Fig. S4. (*A*) In vitro deubiquitination assay of RCHY1 by SARS-CoV PL^{pro} proteins without (lane 2) and with HIS tag (lane 3). HEK293 cells were cotransfected with GFP–RCHY1, HA-ubiquitin, camodulin1-RFP, and CAMK2D–MycYFP N-expression fusion. At 23 h after transfection, cells were treated with PMA and ionomycin to activate CAMK2D for induction of RCHY1 ubiquitination. Ninety minutes after the treatment, cells were harvested and GFP–RCHY1 protein was purified with GFP-trap_A beads. The purified beads-bound GFP–RCHY1 was subsequently incubated with 10 μM SARS PL^{pro} proteins at 25 °C for 30 min in a buffer containing 10 mM Tris·Cl (pH 7.5), 150 mM NaCl, 0.5 mM EDTA, and 2 μM DTT. After incubation, beads were washed twice with washing buffer. The beads-bound GFP–RCHY1 were finally examined with anti-HA and anti-GFP antibodies in Western blot. (*B*) Deubiquitination assay of the SARS-CoV PL^{pro}. The deubiquitination kinetic assay of the SARS-CoV PL^{pro} was performed in 20 mM Tris·HCl, 150 mM NaCl (pH 7.9), 2 mM DTT at 25 °C. The reaction volume was 50 μL. The 0.025-μM SARS-CoV PL^{pro} was used with different concentrations (1, 2, 4, 8 μM) of the fluorogenic substrate uniquitin-7-amino-4-methylcoumarin (AMC; Boston Biochem). The fluorescence signal generated by AMC release was measured using an Flx800 fluorescence spectrophotometer (BioTek; λ_{ex}: 360 nm; λ_{em}: 460 nm). Reactions were started by adding the protease. A calibration curve was generated via measuring the fluorescence of free AMC in the reaction buffer. Saturation was not observed within a reasonable time unless the ratio of protein to substrate was 1:1 or larger. However, the data could be fit to the Michaelis–Menten equation using the GraphPad Prism program (GraphPad Software). The kinetic assay was performed in duplicates. v, reaction rate ($\mu m^{-1} \cdot min^{-1}$); [E], enzyme concentration (μM).

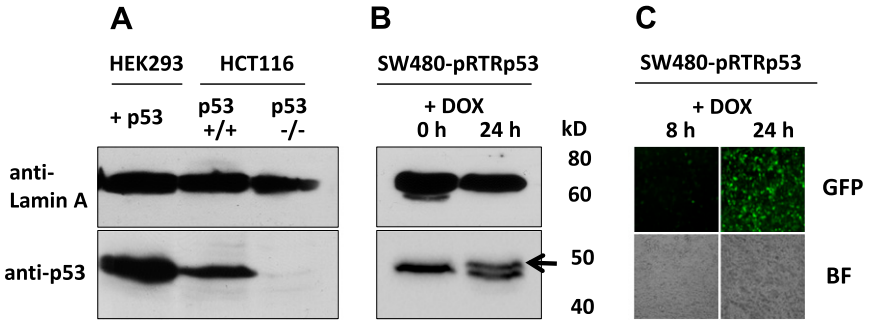

Fig. S5. Characterization of p53 expression in HCT116 $p53^{+/+}$, $p53^{-/-}$, and SW480pRTRp53 cells. (*A*) WB of HEK293 and HCT116$p53^{+/+}$ and $p53^{-/-}$ cells demonstrating lack of expression in p53- negative cells. (*B*) WB of SW480 pRTR cells containing mutated, nonfunctional p53 (single band at 0 h and lower band at 24 h post-DOX induction. The upper band at 24 h + DOX (arrow) represents induced functional p53 protein. (*C*) Fluorescence analysis of WB of SW480 pRTR cells. Functional p53 and GFP are both controlled by the DOX promotor. Expression of both proteins is thus induced by DOX. Conditional expression system: the cell lines SW480 and HCT116 $p53^{+/+}$, $p53^{-/-}$ (44) were kept in DMEM and McCoy's medium, respectively. The pRTR vector (69) harboring a p53–VSV construct is described in ref. 70. Polyclonal SW480/pRTR-p53-VSV cell pools for conditional p53 expression were generated by transfection of the episomal pRTR-p53-VSV expression vector using FuGENE (Roche) and subsequent selection in 2 μg/mL puromycin (Sigma) for 10 d. The percentage of GFP-positive cells was determined 24 h after addition of DOX (Sigma) at a final concentration of 100 ng/mL.

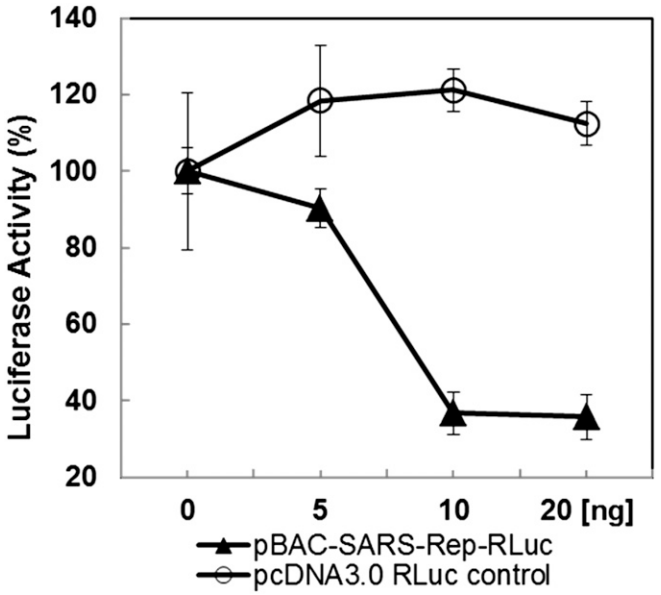

Fig. S6. p53 pressure down-regulates SARS-CoV replicon. Plasmid pBAC-SARS-Rep-R(enilla)luc was used to check the efficiency of genome replication of SARS-CoV replicon under the pressure of p53. pcDNA3.0 RLuc was applied as a control reporter. Effector plasmids were HA-tagged p53 and/or empty HA vectors. The 80-ng reporter plasmids and indicated amount of effector plasmids were cotransfected into HEK293 cells grown in 96-well plates. At 24 h posttransfection, luciferase activity was measured from cell extracts. Experiments were performed in quadruplicates.

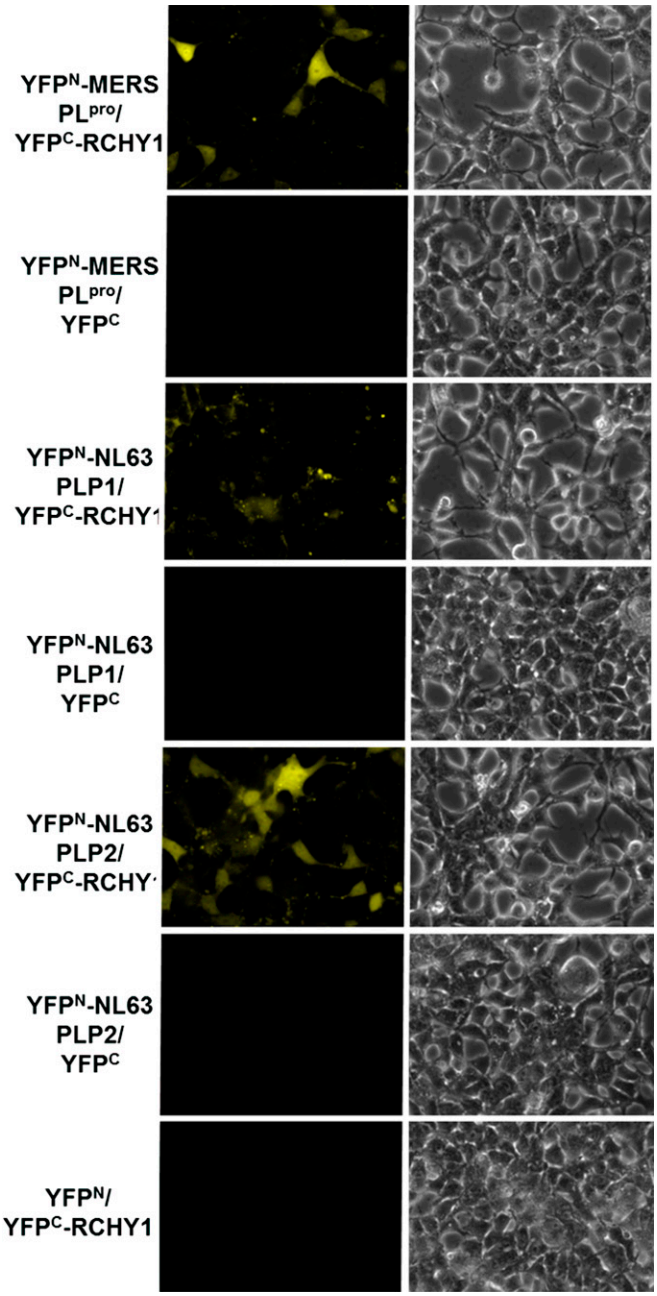

Fig. S7. Split YFP interaction assay of MERS PL^{pro} and NL63 PLP1/2 with RCHY1. YFP^N was fused at the N terminus of MERS PL^{pro} and NL63 PLP1/2, whereas YFP^C was fused at the N terminus of RCHY1. The split-YFP assay was carried out in HEK293 cells as described above.

Table S1. Sequences of primers used for the construction of the various expression plasmids and for qPCR

Primer	Sequence (5′–3′)
c-Myc YFPN(aa 1–155) for	CGC TCA CCG GTA CTA GTA TGG AGC AAA AGT TGA TTT C
c-Myc YFPN(aa 1–155) rev	CTC TGG GCC CTT AAC TCG AGA AGG CCA TGA TAT AGA CGT TG
HA YFPC(aa 156–239) for	GAG AGA CCG GTA CTA GTA TGT ACC CAT ACG ATG TTC C
HA YFPC(aa 156–239) rev	ATA AGG GCC CTT AAC TCG AGA ACT TGT ACA GCT CGT CCA TG
RFP for	CGC TCA CCG GTA CTA GTA TGG TGT CTA AGG GCG AAG AGC
RFP rev	CTC TGG GCC CTT AAC TCG AGA AAT TAA GTT TGT GCC CCA G
GFP for	TAT AGA CCG GTA CTA GTA TGA GCG GGG GCG AGG AGC TGT TC
GFP rev	ATA AGG GCC CTT AAC TCG AGA ACA GCT CGT CCA TGC CGT GG
SUD fl/SUD_N/SUD_NM/SUD–PL^{pro} for	GGG GAC AAG TTT GTA CAA AAA AGC AGG CTC CGC CAT GAA AAT TAA GGC CTG CAT TGA TGA GG
SUD fl/SUD_MC rev	GGGGACCACTTTGTACAAGAAAGCTGGGTCTCMGGATAAGAGACTCTTTAGTTTGTCAAGTGAAAGAAC
SUD_N rev	GGGGACCACTTTGTACAAGAAAGCTGGGTCTCMTAGAATCTCTTCCTTAGCATTAGGTGCTTC
SUD_M/SUD_NM rev	GGGGACCACTTTGTACAAGAAAGCTGGGTCTCMTGATGACGAAGTGAGGTATCCATTATATGTAG
SUD_M/SUD_MC for	GGGGACAAGTTTGTACAAAAAAGCAGGCTCCGCCATGAATTTGAGAGAAATGCTTGCTCATGCTGAAG
SARS PL^{pro} for	GGG GAC AAG TTT GTA CAA AAA AGC AGG CTC CGC CAT G GAGGTTAAGACTATAAAAGTGTTCACAAC
SARS PL^{pro}/SUD–PL^{pro} rev	GGG GAC CAC TTT GTA CAA GAA AGC TGG GTC TCM ATACGACACAGGCTTGATGGTTGTAGTG
MERS MC domain for	GGC GAC AAG TTT GTA CAA AAA AGC AGG CTT CGC CAT G ATTCCACAGAGTTTGACTTTTTCATATGATGG
MERS MC domain rev	GAG GAC CAC TTT GTA CAA GAA AGC TGG GTC TCM CTGCTGTGTCGTGCGTGAATCCAAATACGCACG
RCHY1 fl/aa 1–144 for	TTC TAC AAG TTT GTA CAA AAA AGC AGG CTT CGC CAT G GCGGCGACGGCCCGGGAAGATGGCGC
RCHY1 aa 95–144/ RCHY1 aa 95–261/RCHY1 qPCR for	GGG GAC AAG TTT GTA CAA AAA AGC AGG CTT CGC CAT G AAAGATAAGAAGCAGTATCACTGTGAAAAC
RCHY1 aa 1–144/RCHY1 aa 95–144/ RCHY1 qPCR rev	GGG GAC CAC TTT GTA CAA GAA AGC TGG GTC TCM ATTCTGTTGGGACACATTTTCAATACAC
RCHY1 fl/RCHY1 aa 95–261 rev	GGG GAC CAC TTT GTA CAA GAA AGC TGG GTC TCM TTGCTGATCCAGTGAAATTCTACGTCCTCC
Ubiquitin for	GGG GAC AAG TTT GTA CAA AAA AGC AGG CTT CGC CAT G CAGATCTTCGTGAAGACTCTGACTGG
Ubiquitin rev	ATT GAC CAC TTT GTA CAA GAA AGC TGG GTC TCM CCCACCTCTGAGACGGAGCACCAGGTGCAG
β-actin qPCR for	ATA TAG GCC GTC TTC CCC TCC ATC G
β-actin qPCR rev	ATG GAG TCC ATC ACG ATG CCA GTG
MERS PL^{pro} for	GGG GAC AAG TTT GTA CAA AAA AGC AGG CTC CGC CAT GCAGTTAACAATCGAAGTCTTAGTGACTGTCG
MERS PL^{pro} rev	GGG GAC CAC TTT GTA CAA GAA AGC TGG GTC TCAATCGCTACTGTATTTTTGGCCGGGG
NL63 PLP1 for	GGG GAC AAG TTT GTA CAA AAA AGC AGG CTC CGC CATGGAACAACCTTTTGAAGAAGTTGAACATGTGC
NL63 PLP1 rev	GGG GAC CAC TTT GTA CAA GAA AGC TGG GTC TCA ATAATGACCAGAACCCTTAACACC
NL63 PLP2 for	CC G GGG ACA AGT TTG TAC AAA AAA GCA GGC TCC GCC ATGAAG AAT GAT AAT GTA GTT TTG AAA ATT ACT G
NL63 PLP2 rev	GGG GAC CAC TTT GTA CAA GAA AGC TGG GTC TCA ACTAACAATTGTTGGAACATTAGATGTTAC

aa, amino acids; for, forward; rev, reverse.